3.0 DISTFW-NLFIT Rainfall-Runoff Model

3.1 Introduction

The movement of water via surface and sub-surface mechanisms on slopes is a function of rainfall intensity, vegetation, slope length and form, and soil properties.

The generally accepted mechanisms for water movement on slopes are considered to be Hortonian and Saturated Overland Flow, and unsaturated and saturated throughflow, which are illustrated in Figure 3.1.1.

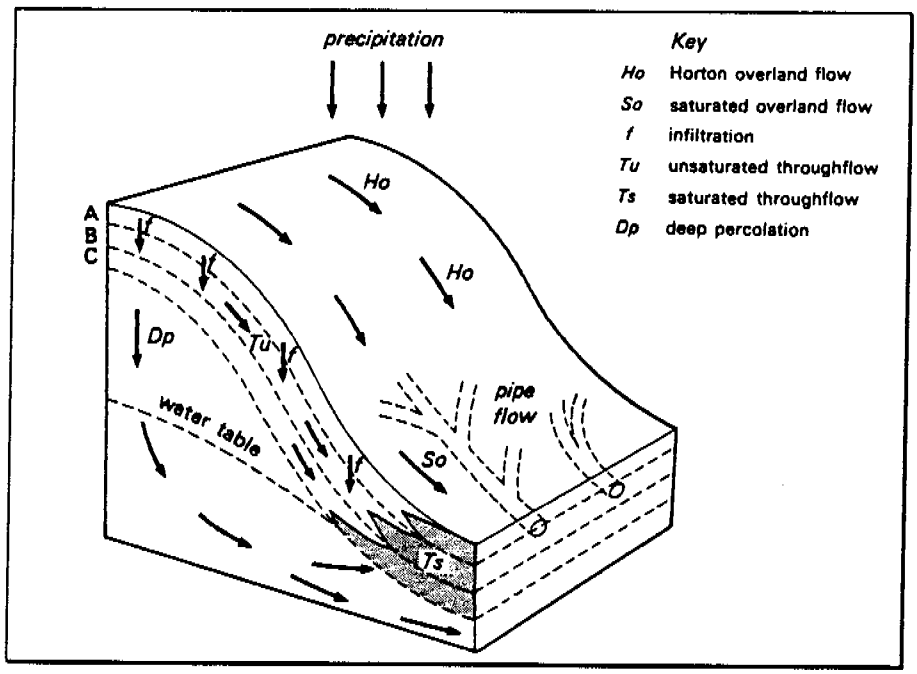

Figure 3.1.1: Numerous mechanisms for water movement exist on hill-slopes including overland and subsurface pathways (after Gerrard, 1981).

The quantity and intensity of surface run-off is a major function governing sediment transportation, thus the accuracy of the estimation of surface run-off is important (Willgoose and Riley, 1993).

The hydrology model utilised in this study and in previous related work on the NWRD (Willgoose and Riley, 1993; Saynor *et al*, 1995; and Evans *et al*, 1996) and in the Tin Camp Creek area (Moliere *et al*, 1996) is the rainfall-runoff model, DISTFW (Willgoose *et al*, 1995). DISTFW, as in previous studies on the NWRD and in Tin Camp Creek, was calibrated to hydrologic and hyetographic field data collected from the natural site.

The DISTFW model which was extended to use digital terrain elevation data (Willgoose *et al*, 1995), is based on the Field-Williams model one-dimensional kinematic wave flood routing model (Field and Williams, 1987). The model was originally called the generalised kinematic catchment model (GKCM) and is a runoff-routing model which has a conceptually more sound basis than other similar models widely used in Australia, namely RORB, and RAFTS, (Kuczera, 1996).

The DISTFW conceptual rainfall-runoff model includes a number of features;

- Flow from surface storage to a channel,
- Flow from groundwater storage to a channel,
- Non-linear storage of water on the hillslope surface,
- Philip infiltration from surface storage to a linear groundwater store, and
- Run-off routing down a channel by use of the kinematic wave.

(Willgoose and Riley, 1995)

The DISTFW rainfall runoff model can be divided into four modules; non-linear surface storage, kinematic wave hillslope routing and channel routing, and linear groundwater storage (Figure 3.1.2). Detailed evaluation of each module of DISTFW is presented in Section 3.2.

The DISTFW-NLFIT model can be used for a standard sub-catchment, a constant width plot, or a DTM based catchment (Willgoose *et al*, 1995). The current study involved a constant width 20 metre by 30 metre rectangular field plot, and the model was adjusted accordingly.

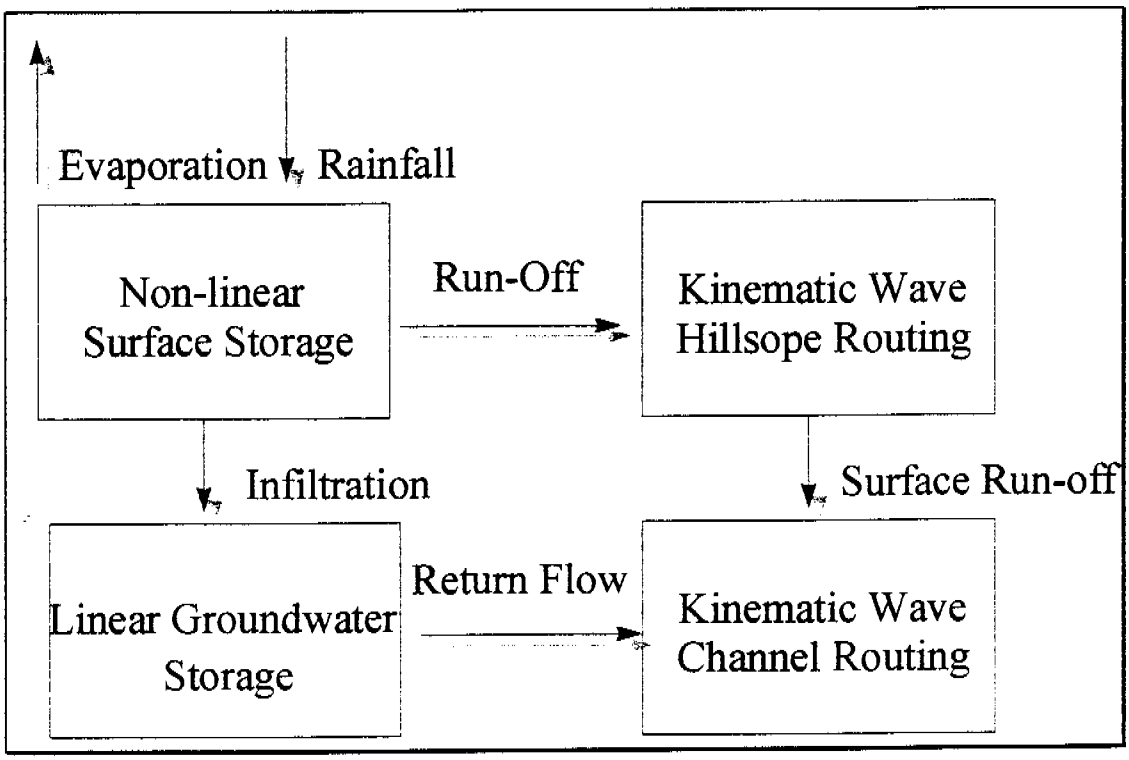

Figure 3.1.2: Four module conceptual arrangement of the rainfall-runoff model, DISTFW, incorporating non-linear surface and linear groundwater storage, and kinematic wave hillslope and channel routing (after Willgoose *et al*, 1995).

3.2 DISTFW-NLFIT

An evaluation of the DISTFW-NLFIT model can be divided into an examination of the processes of infiltration, the routing of overland flow, the routing of sub-surface flow, and channel routing using the kinematic wave approximation.

3.2.1 Infiltration

Gerrard (1981) defined infiltration as the process of water entering the soil, and infiltration capacity as the maximum flux of water across the soil surface. The infiltration properties of the soil tend to govern the volume of surface run-off leaving a catchment (Willgoose and Kuczera, 1995).

A typical infiltration rate curve for a soil under ponded conditions, will feature a period of rapid infiltration followed by an asymptotic decrease until the infiltration rate approaches the infiltration capacity of the soil. Figure 3.2.1 illustrates the infiltration rate of various soils under ponded conditions with respect to time.

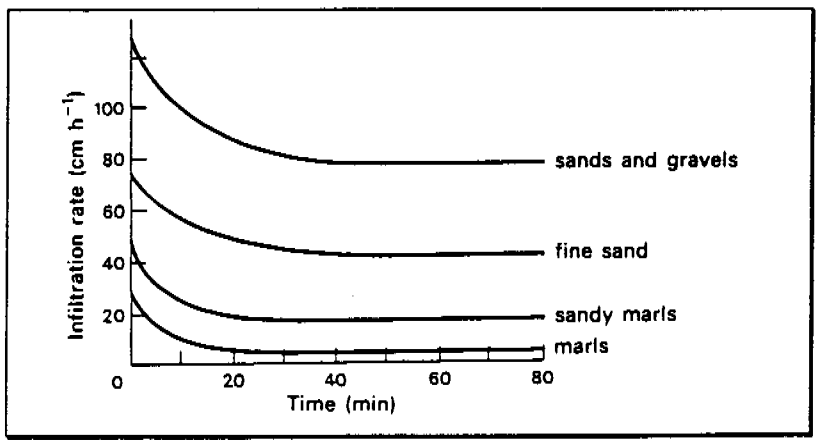

Figure 3.2.1: Typical infiltration rate curves for different soil matrix compositions under ponded infiltration (Gerrard, 1981).

Comparison of the ponded infiltration rate curves for the different soil types featured Figure 3.2.1, highlights that there is only a linear difference between them.

Bodman and Coleman (1943; cited in Gerrard, 1981) divided a typical soil profile into three components in an attempt to quantify the asymptotic behaviour of ponded infiltration rate curves similar to those illustrated in Figure 3.2.1.

Bodman and Coleman postulated that;

- The upper portion of the wetted soil matrix, is merely a transmission zone, which only conducts water from the surface, as it is completely saturated.

- The middle portion of the soil matrix comprises an intermediate zone where the moisture gradient increases with depth.

- The final component of the soil matrix, is the irregular surface of the wetting front, which is characterised by a very high potential moisture gradient.

There are a number of models that attempt to emulate ponded infiltration, namely the Green and Ampt, Kostiakov, Horton, and Philip models (Gerrard, 1981).

There is a clear distinction with infiltration rate behaviour under ponding and non-ponding conditions. Thorne (cited in Kirkby and Morgan, 1980) noted that if the rainfall intensity subjected to a soil is lower than its maximum infiltration under ponded conditions, then non-ponded and pre-ponded infiltration will be prevalent. Figure 3.2.2 illustrates the division of infiltration into four different types; pre-ponding, non-ponding, ponding, and flooding infiltration.

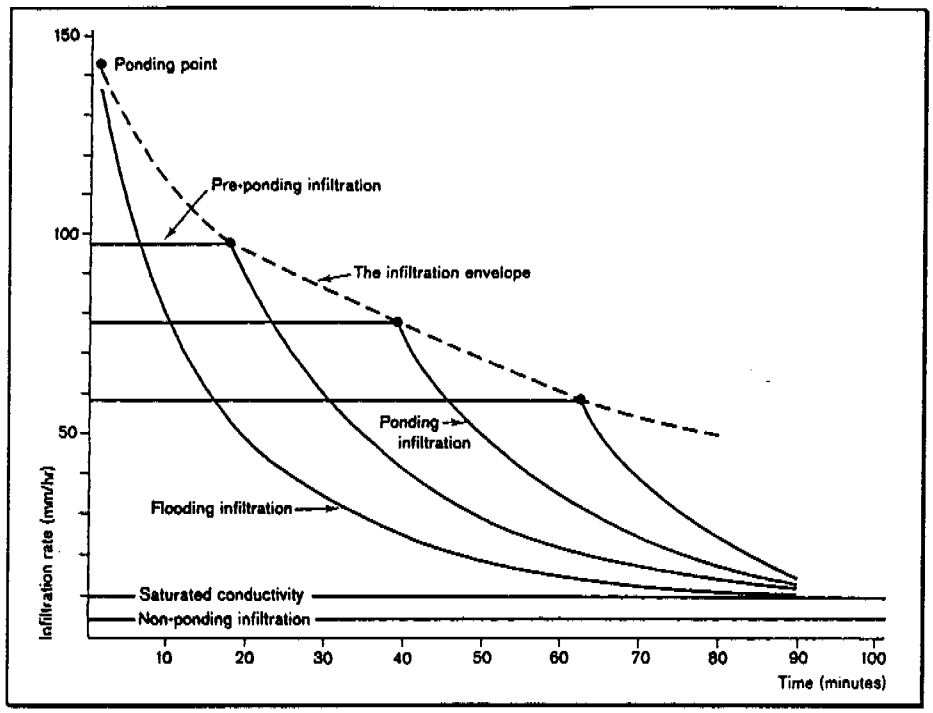

Figure 3.2.2: The infiltration envelope highlighted in this Figure, defines the time to ponding for rainfalls of different hypothetical intensities (Smith, 1972; cited in Kirkby and Morgan,1980).

The infiltration rate, 'i', (m/s), of rainfall into the soil matrix that is modelled in DISTFW, can be divided into the two processes, ponded and non-ponded, at any timestep, Δt, (Equation 3.2.1), (Kuczera, 1996).

$$i = \begin{cases} f & \text{if ponding occurs, namely } p\Delta t + h^s \geq f\Delta t \\ p + \dfrac{h^s}{\Delta t} & \text{otherwise} \end{cases} \qquad (3.2.1)$$

where

i = Infiltration rate, (m/s),

f = Soil infiltration capacity, (m/s),

h^s = Average depth of surface storage, (m),

p = Rainfall intensity, (m/s), and

Δt = Timestep, (s).

Under conditions of ponding, the DISTFW model assumes that the infiltration capacity of the soil is governed by the Philip's equation (Equation 3.2.2), which takes the form of the flooding infiltration rate curve of Figure 3.2.2.

$$f = \frac{S_\phi}{2\sqrt{t}} + \phi \qquad (3.2.2)$$

where

S_ϕ = Sorptivity, ($m/s^{1/2}$),

ϕ = Continuing loss rate, (m/s), and

t = Time since commencement of ponding, (s).

Field and Williams (1987) noted that sorptivity is a soil parameter which describes the initial dryness of the soil, and that the continuing loss rate, is a parameter that represents the saturated hydraulic conductivity of the soil.

Equation (3.2.2) has the underlying assumption that a condition of ponding will be prevalent throughout a storm event, which is not the case in reality. A time compression algorithm was utilised to find an approximate solution to this problem, such that 'f', the soil infiltration capacity, (m/s), can be expressed as a function of the cumulative infiltrated depth, 'F', (m), (Equation 3.2.3), (Field and Williams, 1987).

$$F = \int_0^t [\frac{1}{2} S_\phi V^{-\frac{1}{2}} + \phi] dv$$

$$F = S_\phi t^{\frac{1}{2}} + \phi t \qquad (3.2.3)$$

where

F = Cumulative infiltrated depth, (m), and

V = Velocity of the wetting front, (m/s).

Willgoose and Kuczera (1995) noted that the instantaneous infiltration rate, 'f', (m/s), as a function of the cumulative infiltration, 'F', (m), from DISTFW can be rearranged as Equation 3.2.4.

$$f = \phi + \frac{S_\phi^2}{4F}\left(1 + \left(1 + \left(\frac{4F\phi}{S_\phi^2}\right)\right)^{\frac{1}{2}}\right) \qquad (3.2.4)$$

Rainfall that does not infiltrate and overcomes depression storage becomes overland flow, which is modelled as a Hortonian process in DISTFW. Willgoose and Kuczera (1995) stressed that changes in infiltration rates mainly influence the volume of run-off that occurs at the outlet of the catchment.

The process of rainfall becoming overland flow, is schematically illustrated in Figure 3.2.3 (Fetter, 1994).

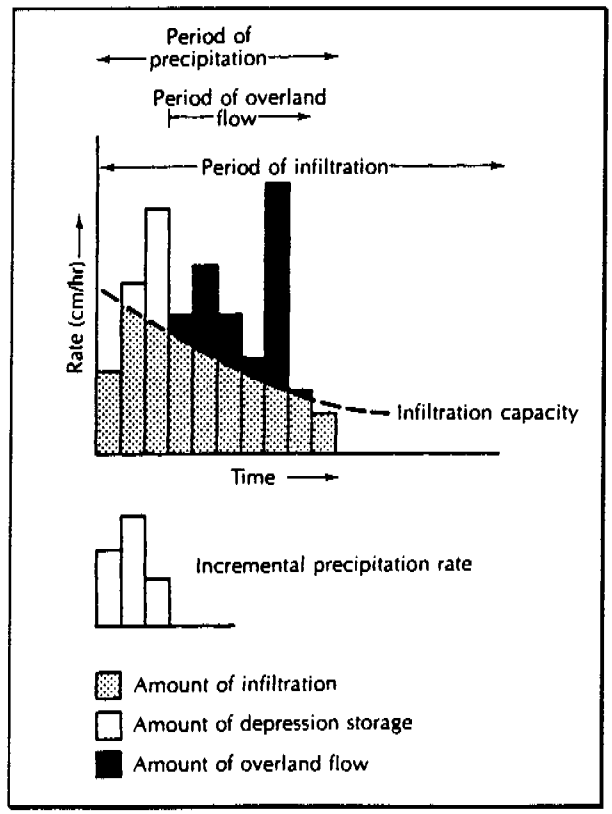

Figure 3.2.3: Incremental precipitation rate and its dissociation into amounts of infiltration, depression storage, and overland flow (Fetter, 1994).

Figure 3.2.3 illustrates that overland flow will continue past the point of the cessation of rainfall, and that infiltration will continue past the point of the cessation of overland flow.

3.2.2 Routing of Overland Flow - Hillslope Run-off

Surface overland flow modelled in DISTFW is based on the concept of Hortonian overland flow. Field and Williams (1987) noted that this type of flow mechanism can only be observed on disturbed or scantly vegetated surfaces. They continued that on natural undisturbed surfaces, overland flow is likely to be dominated by saturation overland flow rather than Hortonian flow. They concluded however that, although there is a conceptual limitation between modelling saturation overland flow as Hortonian flow, the rainfall runoff model can be successfully calibrated to catchments where there is domination of the saturation overland flow process due to similarities between the processes.

Willgoose and Kuczera (1995) emphasised that the original Field-Williams model was designed to be an event model which was extended to model continuous flow series through the addition of infiltration recovery and evaporation components to Equation 3.2.4 in DISTFW, which is illustrated in the four module schematic of the model (Figure 3.1.2).

As the overland flow moves down-slope it encounters resistance which establishes temporary storage, which results in rainfall in excess of the maximum infiltration capacity, being delayed and attenuated (Kuczera, 1996). Field and Williams (1987) noted that DISTFW approximates the dynamics of the delay and attenuation of excess rainfall by utilising a non-linear level-pool routing mechanism.

Willgoose and Kuczera (1995) noted the non-linear level-pool routing mechanism can be defined with respect to the discharge per unit area of surface storage, 's^s', (m/s), as Equation (3.2.5).

$$s^s = \left(\frac{h^s}{C_s B^\gamma} \right)^{\frac{1}{\gamma}} \qquad (3.2.5)$$

where

B = Width of the catchment element, (m),

C_s = Surface supply parameter, ($m^{(1-2\gamma)}s^\gamma$),

h^s = Average depth of surface storage, (m), and

γ = Parameter to be determined from observations on actual catchments.

Field and Williams (1987) emphasised that the parameters C_s and γ, can only be estimated through calibration to observed storm events. Willgoose and Kuczera (1995) noted that Equation (3.2.5) can be used to model surface depressions such as deep rip patterns on rehabilitated mine surfaces.

Figure 3.2.4 illustrates the principle of the delay and attenuation of rainfall excess in the form of temporary storage of surface water on a hillslope.

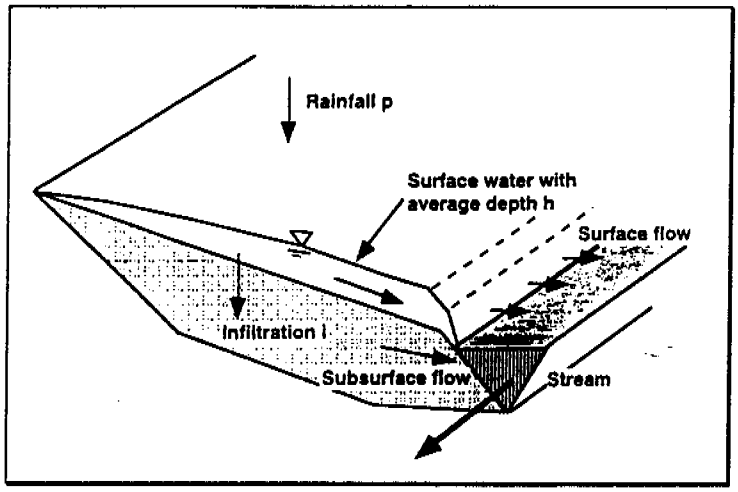

Figure 3.2.4: A schematic of a hillslope which illustrates the principal of temporary storage of surface run-off, infiltration and subsurface flow (Kuczera 1996).

Field and Williams (1987) noted that a mass balance may be applied to surface water moving in an overland flow manner toward a 'stream', illustrated in Figure 3.2.4. Figure 3.2.4 also highlights that the non-linear surface storage of water is the source of water for the routing component, the kinematic wave (Willgoose and Kuczera, 1995).

3.2.3 Routing of Channel Flow

Chaudhry (1993) noted that flood routing can be referred to as the computation of the height and velocity of a flood wave as it propagates in a body of water (channel, lake, stream, reservoir etc.). Finnegan (1993) observed that the routing of channel flow is developed from theories of unsteady flow, which generally involve translatory waves. These translatory waves are gravity waves that occur within channels that cause particles of fluid to be displaced in a direction parallel to the flow. Chaudhry (1993) noted that the simultaneous solving of the continuity equation with a simplified form of the momentum equation assuming steady uniform conditions, is referred to as the kinematic routing procedure.

Derivation of the kinematic wave channel routing component of the DISTFW model can be found in Field and Williams (1987), Finnegan (1993), and Kuczera (1996).

The conveyance properties of hillslopes and channels in DISTFW differ and are permitted to change with respect to discharge (Willgoose and Kuczera, 1995). They continued that changes in those conveyance properties allows DISTFW to predict behaviour of overbank flow regions in flooded rills or channels.

The Manning's equation is utilised to determine discharge, coupled with the kinematic wave assumption that the pressure and inertia terms of the momentum equation are negligible when compared to the gravity and friction terms. If the slope is not so mild that the pressure term becomes appreciable, not less than approximately 0.05%, and that the translatory wave does not rise and fall too quickly (ie the assumption of negligible vertical acceleration holds) then the assumption that the friction slope is equal to the bed slope is valid.

Equation (3.2.6) represents Manning's equation with the assumption that the friction slope, 'S_f' is equal to the bed slope, 'S_0'.

$$q = \frac{1}{n}\left(R^{\frac{2}{3}}S^{\frac{1}{2}}P\right) \qquad (3.2.6)$$

where

n = Manning's roughness coefficient,

q = Discharge per unit width of hillslope, ($m^3/s/m$),

R = Hydraulic radius, (m),

P = Wetted perimeter, (m), and

S = Bed slope, (m/m).

As the hydraulic radius is equal to the cross sectional area of flow divided by the wetted perimeter, then Equation (3.2.6) can be re-expressed as Equation (3.2.7).

$$q = \frac{1}{n}\left(A^{\frac{2}{3}} S^{\frac{1}{2}} P^{-\frac{2}{3}}\right) \qquad (3.2.7)$$

where

A = Cross sectional area of flow, (m^2).

Incorporation of the cross sectional area and wetted perimeter terms of Equation (3.2.7), into the channel conveyance term, 'K', (m^3/s), (Willgoose and Kuczera, 1995), allows the discharge per unit width, 'q', (m^3/s) to be simply stated (Equation 3.2.8).

$$q = KS^{\frac{1}{2}} \qquad (3.2.8)$$

where

K = Channel conveyance, (m^3/s).

The channel conveyance can be approximated by a power law function involving the cross sectional area of flow (Equation 3.2.9), (Willgoose and Kuczera, 1995).

$$K = C_r A^{e_m} \qquad (3.2.9)$$

The parameters C_r and e_m are defined by the flow geometry and surface roughness and have non-dimensional units, but together define the kinematic wave component of DISTFW. It can be observed from Equation (3.2.9), that as the magnitude of C_r increase the rate of discharge also increases.

Figure 3.2.5 illustrates the cross sectional flow geometries of four different overland sheetflow and rillflow profiles.

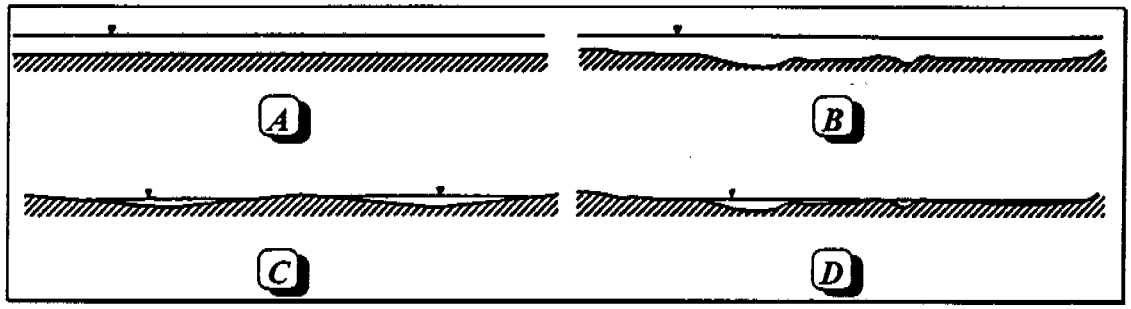

Figure 3.2.5: Combination of four different cross sectional profiles illustrating A) Constant depth sheet flow, B) Irregular depth sheet flow, C) Triangular rill flow, and D) Irregular depth rill flow (after Willgoose and Kuczera, 1995).

It can be observed from Figure 3.2.5 that cases '*A*' and '*B*', are cross sectional profiles which exhibit sheet flow. Surface water in these two cases, has a constant or irregular depth over the entire width of the hillslope (Willgoose and Kuczera, 1995), and the cross sectional area is proportional to the wetted perimeter. They continue that if, with an increase in discharge, the wetted perimeter per unit width remains virtually constant, then C_r and e_m can be defined as Equation (3.2.10).

$$C_r = \frac{1}{P^{0.67}n} \qquad e_m = 1.67 \tag{3.2.10}$$

It can be observed from Figure 3.2.5 that the cross sectional profile for case '*C*', is one of triangular rillflow. Surface water in this case does not have a constant or irregular depth over the entire width of the hillslope, rather the flow is concentrated in rivulets, that is, only a small proportion of the hillslope is contributing to surface runoff (Willgoose and Kuczera, 1995).

They continued that in this case, the cross sectional area is proportional to the square of the wetted perimeter, and for a channel with a side slope of 1:α and 'N' number of rills per unit width, C_r and e_m can be defined as Equation (3.2.11).

$$C_r = N\left(\frac{\left(\frac{\alpha}{4(1+\alpha^2)}\right)^{0.33}}{n}\right) \qquad e_m = 1.33 \qquad (3.2.11)$$

The final cross sectional profile to be considered is that of a natural surface, case '***D***' (Figure 3.2.5). Willgoose and Kuczera (1995) noted that C_r and e_m can be derived from the analysis of cross sections that are perpendicular to the direction of flow. The relationship between the cross sectional area and the wetted perimeter for a natural field plot is reported in Equation (3.2.12), (derived by Parsons, Abrahams, and Luk, 1990; cited in Willgoose and Kuczera, 1995).

$$A = 0.0076P^{1.49} \quad R^2 = 0.88$$
$$C_r = \frac{0.113}{n} \qquad e_m = 1.21 \qquad (3.2.12)$$

Willgoose and Kuczera (1995) emphasised that a kinematic wave response close to linearity would be expected with surface irregularities rather than the sheetflow kinematic wave assumption generally accepted in hydrologic models such as KINCAT (Field and Williams, 1987).

3.3 DISTFW Data Requirements

The DISTFW-NLFIT package utilised in this study is the same as used in previous studies on the NWRD of ERARM, (Willgoose and Riley, 1993; and Saynor *et al*, 1995) and in the Tin Camp Creek area (Moliere *et al,* 1996).

A UNIDATA data-logger, provided by ERAES, was programmed utilising a connected laptop computer and accompanying data-logger software. The data-logger was programmed to accept two channels of input; a tipping bucket raingauge and a water level sensing device (capacitance rod), (Section 2.0).

A laboratory calibration experiment was conducted prior to the installation of the capacitance rod on-site to establish a relationship between the capacitance reading, (Hz), and the relative water level, (mm), (Figure 3.3.1).

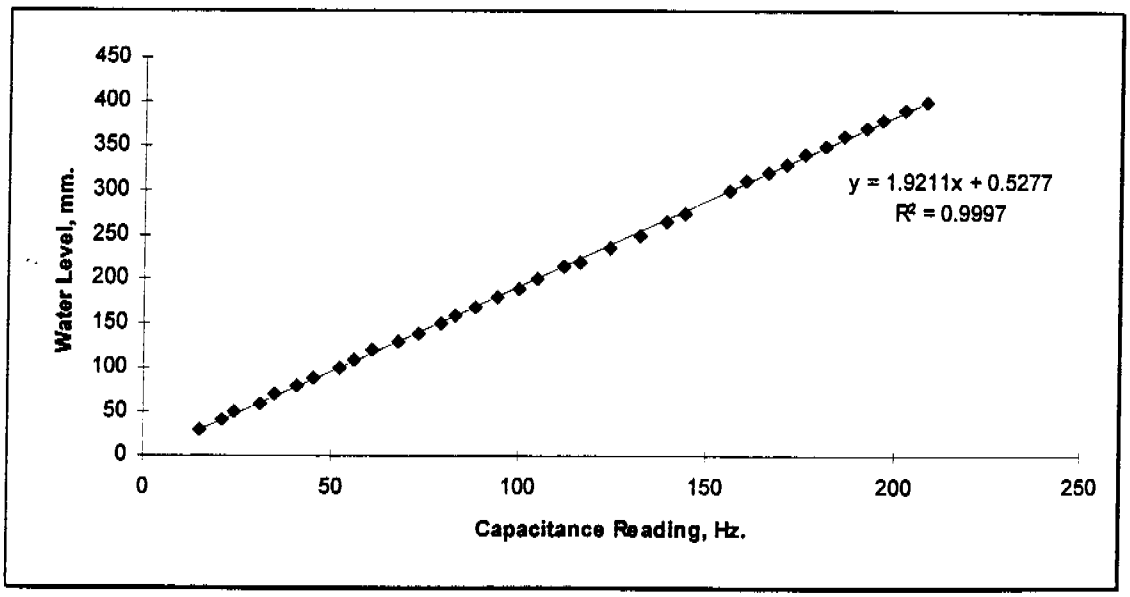

Figure 3.3.1: Regression analysis of the results obtained from the calibration experiment performed on the water level sensing device (capacitance rod), prior to installation on-site.

In previous studies it was suggested that readings from the capacitance rod had a dependency upon water temperature within the stilling well. A separate experiment was undertaken to evaluate the effect of stilling well water temperature but was not reported, and found no temperature dependency of readings from the capacitance rod utilised for the natural site.

The water level, (m), as a function of resistance reading, (Hz), is presented as Equation (3.3.1).

$$\text{Water Level(m)} = 1.9211 \times \text{Reading(Hz)} + 0.5277 \quad (r^2 = 1.0) \quad (3.3.1)$$

The rainfall data recorded by the data-logger was stored in the form of the number of cumulative tips that had occurred since the previous logger reset, with an accompanying time signature. The runoff data recorded, was in the form of a resistance value, (Hz), from the capacitance rod, which varied according to the water height, (m), moving through the hydraulic control structure. Figure 3.3.2, illustrates an extract of a raw data file, illustrating the two data sources; rainfall and runoff.

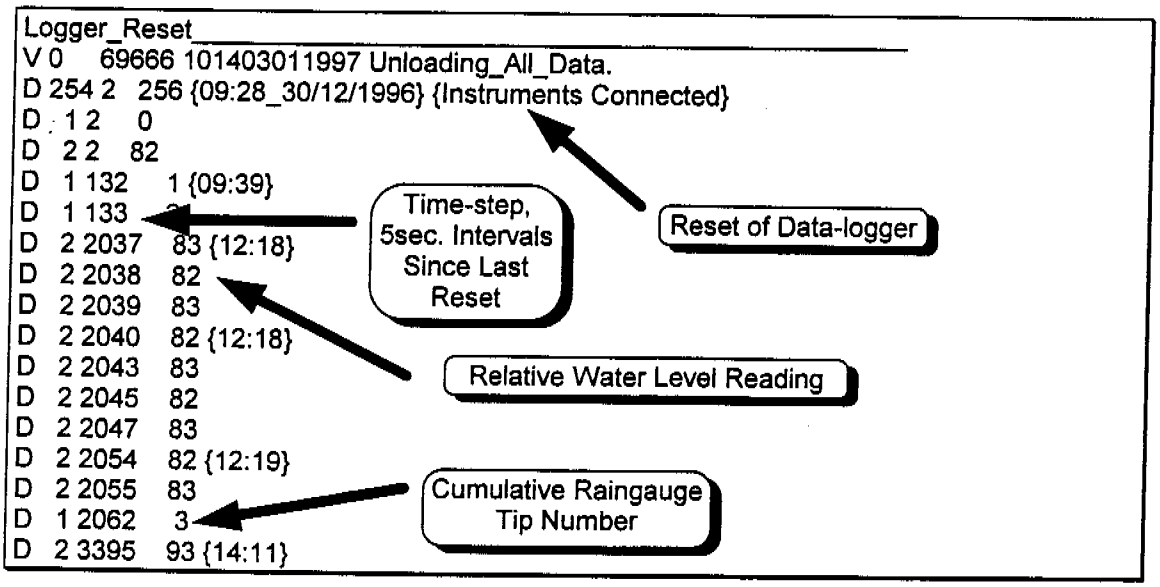

Figure 3.3.2: An extract from a raw data file unloaded from the UNIDATA data-logger highlighting the number of tips from the electronic raingauge, and the water level via a capacitance reading. It should be noted that the number in the column after the 'D', representing a data-entry line, represents the channel that each device was connected to within the data-logger.

Raw rainfall and runoff data similar to the extract (Figure 3.3.2), was obtained from the UNIDATA data-logger at regular intervals by transferring data to a laptop computer. The data-logger was reset with the accompanying software and re-sealed. The discharge, (m^3/s), and cumulative rainfall, (mm), data was arranged in DISTFW rainfall and runoff file format.

The DISTFW-NLFIT model required data pertaining to the topography of the catchment and the runoff response from the catchment, under certain rainfall.

The 'Field Williams' input file (a *.fw file), could be considered as the controlling file, and containing information on; the sub-catchment number and their relative size; upstream/downstream elevation; linkage from one sub-catchment to another; storm duration; rainfall and runoff input file names; and erosion parameters and calibration data. It should be noted that the erosion component of the DISTFW model was not utilised in this study. Further discussion pertaining to the prediction of erosion from the field plot are considered in Section 4.0 of this report.

The topographical characteristics of the field plot were determined by a survey with a TopCon total station theodolite. Figure 3.3.3 highlights the division of the field plot into ten equal sub-catchments that were entered into the 'Field Williams' input file.

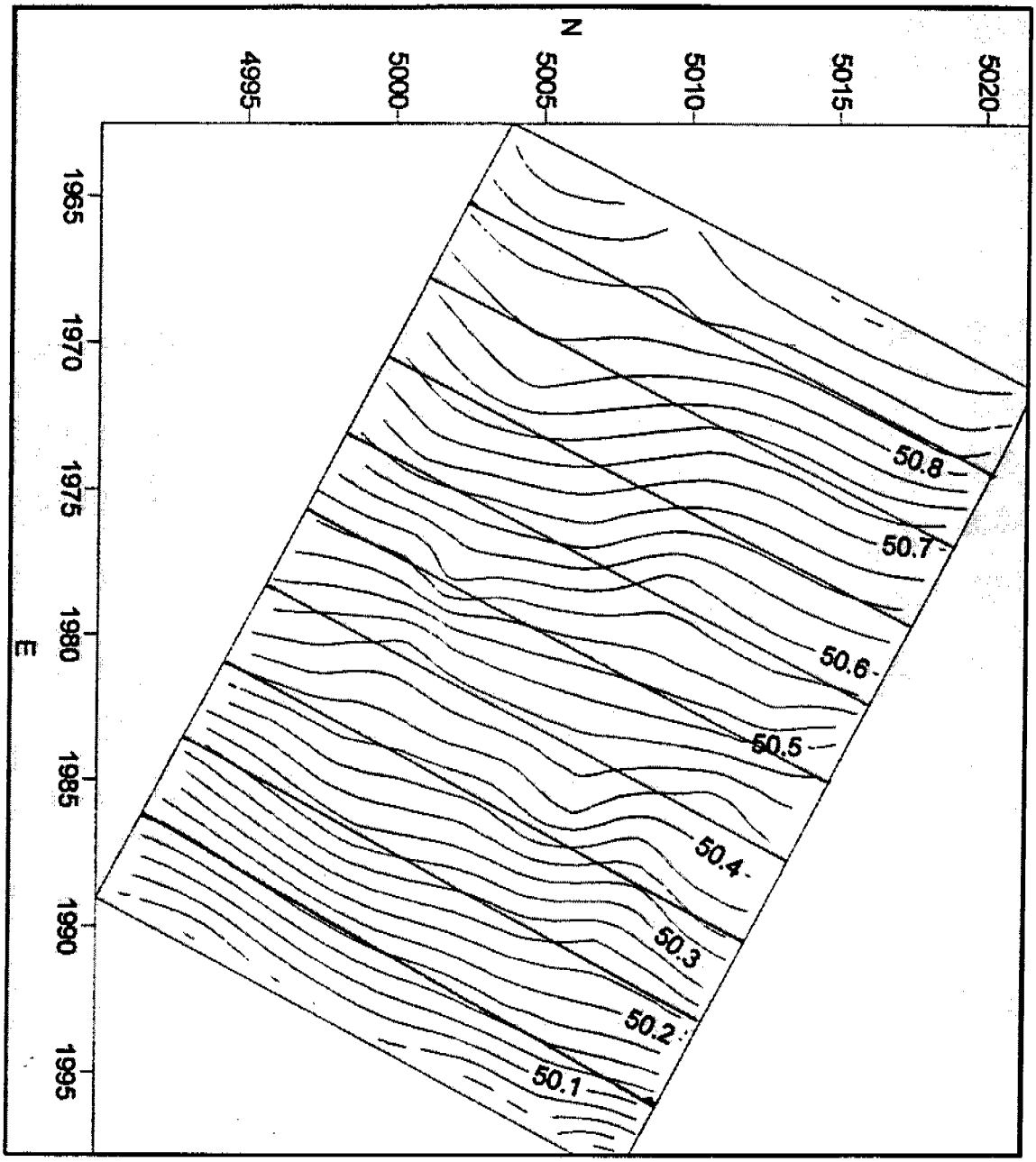

Figure 3.3.3: The 30 m in length, and 20 m in width, 600 m^2 field plot was divided into ten equally proportioned sub-catchments and upstream and downstream elevation information was entered into the 'Field Williams' file. The Northing and Eastings including topographic measurements can only be conservative to one another.

Each sub-catchment had a length of 3 metres and a width of 20 metres, with a total area of 60 square metres. The 'Field Williams' input file was especially modified to accept sub-catchments that were connected together in the form of a field plot, as there was no specific main channel for discharge as in a normal catchment (Willgoose *et al*, 1995).

The typical features of a 'Field Williams' file are illustrated in Figure 3.3.4.

```
Data file is for a rainfall simulation plot (plot version)
RUMPIT 1 large scale plot Monitoring
01/01/97 1550hrs
PLOT
# No of elements, No of reservoirs, no of u/S elements
   10          0          1
# No of U/S element draining into D/S elements
#
# zero time (hrs), timestep (minutes), time of duration of storm (hrs)
#
0 0.05 1.9
# ----------------------------
# OUTPUT PARAMETERS
# ----------------------------
# no of pts for output discharge,psteps
1 1
# subareas at which discharge requested
10
# maximum discharge on output graph
0.002
#
INCIDENCES
 0  1  2  3  4  5  6  7  8  9
PARAMETERS
# Kind of element
  0
# No Area Length  U/S      D/S    SWSupply Gamma Sorpt Phi GWsupply
#             Elevation Elevation
# ------------------------------------------------------------
  1 60.0 3.0  50.9     50.825    1.0   1.0  1.0 1.0  1.0
  2 60.0 3.0  50.825   50.725    1.0   1.0  1.0 1.0  1.0
  3 60.0 3.0  50.725   50.65     1.0   1.0  1.0 1.0  1.0
  4 60.0 3.0  50.65    50.575    1.0   1.0  1.0 1.0  1.0
  5 60.0 3.0  50.575   50.50     1.0   1.0  1.0 1.0  1.0
  6 60.0 3.0  50.50    50.425    1.0   1.0  1.0 1.0  1.0
  7 60.0 3.0  50.425   50.35     1.0   1.0  1.0 1.0  1.0
  8 60.0 3.0  50.35    50.225    1.0   1.0  1.0 1.0  1.0
  9 60.0 3.0  50.225   50.125    1.0   1.0  1.0 1.0  1.0
  10 60.0 3.0  50.125   50.025    1.0   1.0  1.0 1.0  1.0
# Hillslope and Channel conveyances
#    1st set are hillslope conveyances
#    2nd set are  channel  conveyances
# Element No, No of conveyances
# CR, EM, CONVEY
#
CONVEYANCES
1 2
0.136     1.     0.
0.136     1.     1000.
#
# Parameter Multpliers
# Ch-CR  Ch-EM  SWSupply SWGamma Sorptivity   Phi  GWSupply  timing(sec)
MULTIPLIERS
  7.8   1.33   0.03     0.375 0.00001    6.5    1000.    0.0
1
0.0 0.0
# No of pluvios
RAINFALL #1
   1
CUMPLUVIO 1197.rf
1.00 1.00 1.00 1.00 1.00 1.00 1.00 1.00 1.00 1.00
#  No of known initial flows at stations
INITIALQ
title line 1
title line 2
title line 3
   1
# stations at which flows known and initial flow (cumecs)
  10 0.0
#  No of stations with known inflows
INFLOWQ NONE
#  Hydrograph to calibrate with (no of values )
CALIB #1 1197.ro
END
```

Storm duration and timestep

Subcatchment Topography

Parameter Multipliers

Rainfall Input File Name

Runoff Input File Name

Figure 3.3.4: A typical Field Williams input file, containing topographic information on the field plot, and the rainfall and runoff input file names for a particular storm event.

The rainfall and runoff input files for the DISTFW model, contain the cumulative rainfall, (mm), and discharge at the outlet of the catchment, (m^3/s), respectively. The outlet of the catchment in this case is the PVC discharge trench, as featured in Figure 2.2.2. Every data point in the rainfall and runoff files has a time signature, in decimal hours associated with it. Figures 3.3.5, and 3.3.6 respectively illustrate typical DISTFW rainfall and runoff input data files.

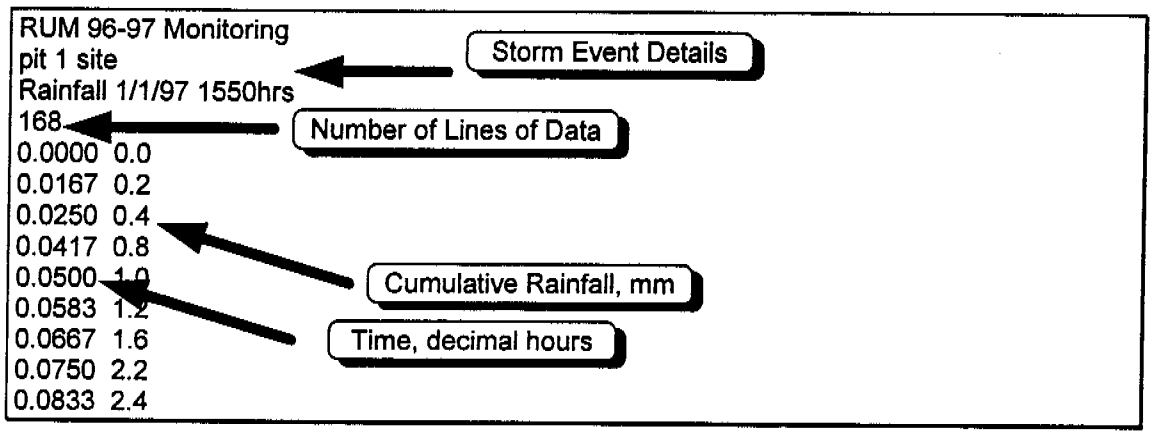

Figure 3.3.5: A DISTFW rainfall input file featuring a title, and cumulative rainfall with accompanying time stamp in decimal hours since the commencement of the event.

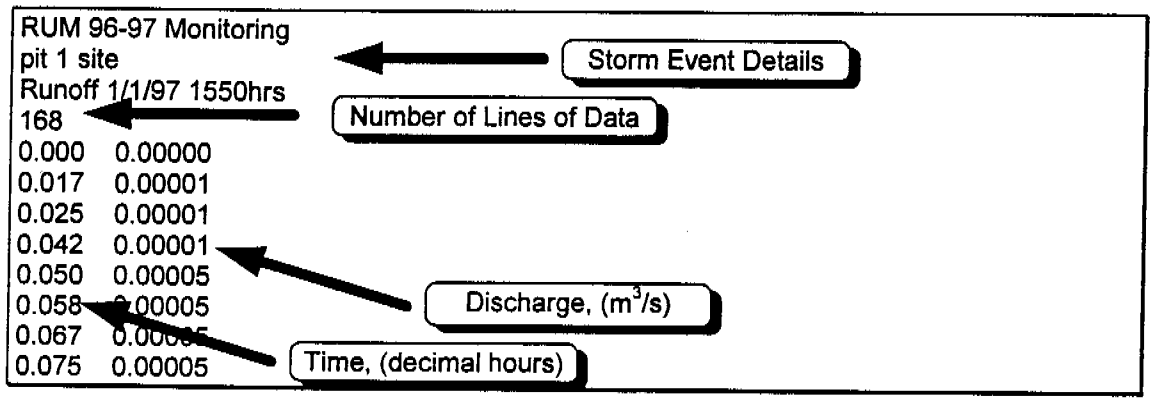

Figure 3.3.6: A DISTFW runoff input file featuring a title, and discharge, (m^3/s), with accompanying time stamp in decimal hours since the commencement of the event.

All DISTFW rainfall, runoff and Field Williams files utilised in this study appear in Appendix 3.A.

3.4 DISTFW-NLFIT Calibration Procedure

The DISTFW model was calibrated according to the procedure outlined in Willgoose *et al* (1995), and Saynor *et al* (1995). The magnitudes and standard deviations of the two kinematic wave parameters, Cr and e_m, and the two infiltration parameters, S_ϕ and ϕ, were primarily of interest in this study.

Parameters were estimated with the DISTFW-NLFIT package by means of a descent method, which evaluated the gradient direction of the response surface at each iteration and progressively stepped in a downhill direction until the objective function reached a minimum (Johnston and Pilgram, 1976). Figure 3.4.1 features the global optimisation of the hypothetical objective function $\psi(\gamma)$, which comprises of a three dimensional response surface with contours of constant of $\psi(\gamma)$ whose magnitude is a function of the two hypothetical parameters, γ_1 and γ_2.

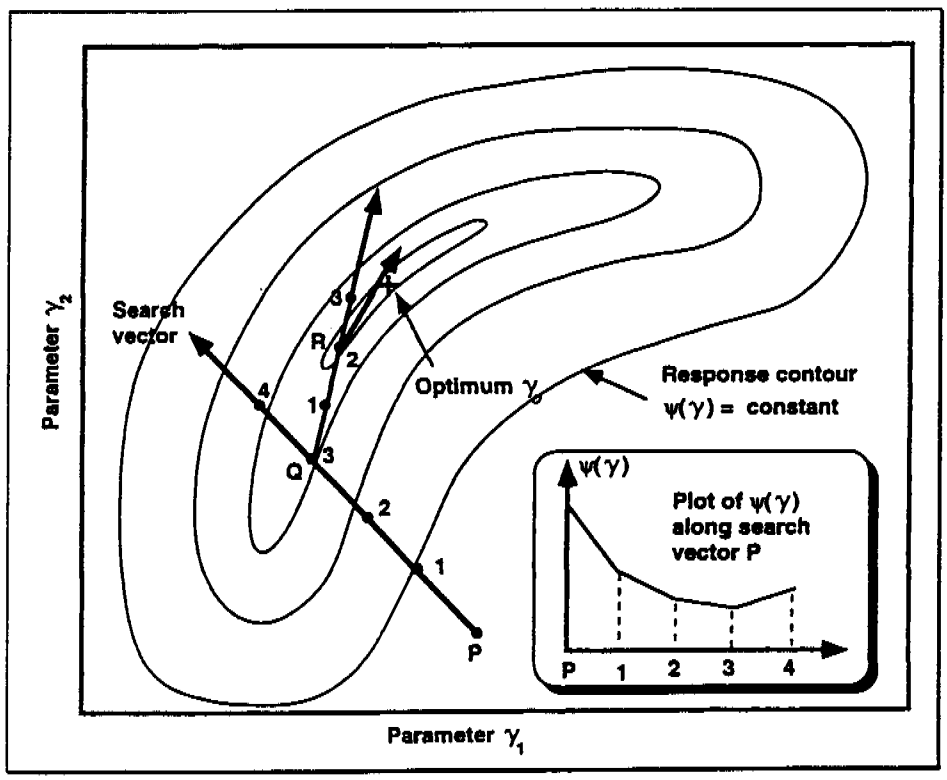

Figure 3.4.1: The global optimisation of the objective function $\psi(\gamma)$, involves the search vector moving in a down-gradient direction until a minimum is reached, denoted by an 'X' (Kuczera, 1994).

The value of parameters from the DISTFW model can be estimated with NLFIT, as illustrated in Figure 3.4.1. Parameters of the DISTFW model include; C_r, e_m, C_s,γ, S_ϕ, ϕ, C_g, '*timing*' and '*initial wetness*'; where C_s is a coefficient and γ is the exponent from the surface storage equation (Equation 3.2.5); and C_g is a coefficient from the groundwater storage equation, which was not considered in the current study; '*timing*' is a factor to account for differences in time between rainfall and runoff data (usually associated with data from different sources); and '*initial wetness*', is only applicable in multiple fitted storm events (where it accounts for differences in catchment response from various states of initial wetness). Only the kinematic wave and infiltrative loss parameters, C_r, e_m, S_ϕ, and ϕ were estimated in this study.

Table 3.4.1, highlights the initial starting values for the parameters utilised in the DISTFW model as recommended in Willgoose *et al* (1995).

Table 3.4.1: DISTFW model parameter initial calibration magnitudes and designation as to whether an estimation of the parameter was sought or whether the parameter's value was permanently fixed.

Parameter	*Magnitude*	*Permanently Fixed*
C_r	10	No
e_m	1.67	No
C_s	0.003	Yes
γ	0.375	Yes
S_ϕ	0.001	No
ϕ	0.001	No
C_g	1000	Yes
Timing	0.001	Yes
Initial Wetness	0.001	Yes

Willgoose and Kuczera (1995) noted that during simulations, only one of the non-linear or kinematic wave stores should be enabled due to parameter identification difficulties that could be encountered. As such the magnitudes of the surface storage parameters of C_s and γ were permanently fixed in this study.

The groundwater storage equation was not considered in this study, as over normal short storm durations groundwater contribution to catchment runoff was negligible.

Willgoose *et al* (1995) noted that due to stability problems associated with the DISTFW model, the parameters of C_r, C_s, S_ϕ, ϕ, and '*initial wetness*', must not have magnitudes less than or equal to 0.0. They continue that if S_ϕ becomes relatively large and is incorporated into the Philip's infiltration model then the root of a negative number will attempt to be found and will cause program instabilities.

The following calibration procedure was adopted due to the severe parameter interactions within the DISTFW model (Willgoose et al, 1995);

- Fit C_r and ϕ, to approximate the timing and volume of the hydrograph,
- Fit S_ϕ and ϕ, to better approximate the volume of the hydrograph,
- Fit C_r and e_m, to achieve a better approximate of the routing of the hydrograph, and
- Fit all parameters, to achieve a polished approximation of the hydrograph.

A least squares error model was chosen initially for each storm event calibration. In many cases, because of a lack of statistical normality in the distribution of errors, a more general error model needed to be adopted. Kuczera (1994) noted that the adequacy of the least squares error model could be evaluated through simple diagnostic residual plots. The DISTFW-NLFIT package utilised in this study incorporated these diagnostic residual plots. Comparisons were made between each error model to determine the one that yielded the most accurate predicted hydrograph compared to that which was observed, and that satisfied the most diagnostic residual plots. Due to the complexity of the statistics associated with the NLFIT package, reference is made to Kuczera (1994) for further information beyond the summary presented in Section 3.5.

3.5 NLFIT-General and Least Squares Error Models

Kuczera (1994) noted that the least squares error model assumes that; the expected value of the random error 'ε_t' is zero; and the variance of 'ε_t' equals a constant 'σ^2'; the errors are statistically independent of each other; and are normally distributed. The least squares error model is summarised as Equation (3.5.1)

$$\varepsilon_t \sim N(0, \sigma^2) \tag{3.5.1}$$

A residual is an estimate of the true random error 'ε_t'. The standardised residual 'Z_t' is defined in Equation (3.5.2) (Kuczera, 1994).

$$Z_t = \frac{\hat{\varepsilon}_t}{\sigma} \tag{3.5.2}$$

Kuczera (1994) continued that if a least squares model is adequate in predicting error, then the standardised residuals should have a normal distribution, $Z_t \sim N(0,1)$. This normal distribution implies that 95% of the 'Z_t' values should fall within the range -2 and 2. If the absolute value of 'Z_t' is beyond 2, then a more general error model should be investigated.

Kuczera (1994) considered the most informative diagnostic output is a plot of predicted response versus standardised residuals, where a randomly scattered pattern is evidence of least squares model adequacy. Figure 3.5.1 illustrates a residual versus predicted response plot for the parameter estimation of storm event occurring on the 1/1/97, utilising a least squares error model.

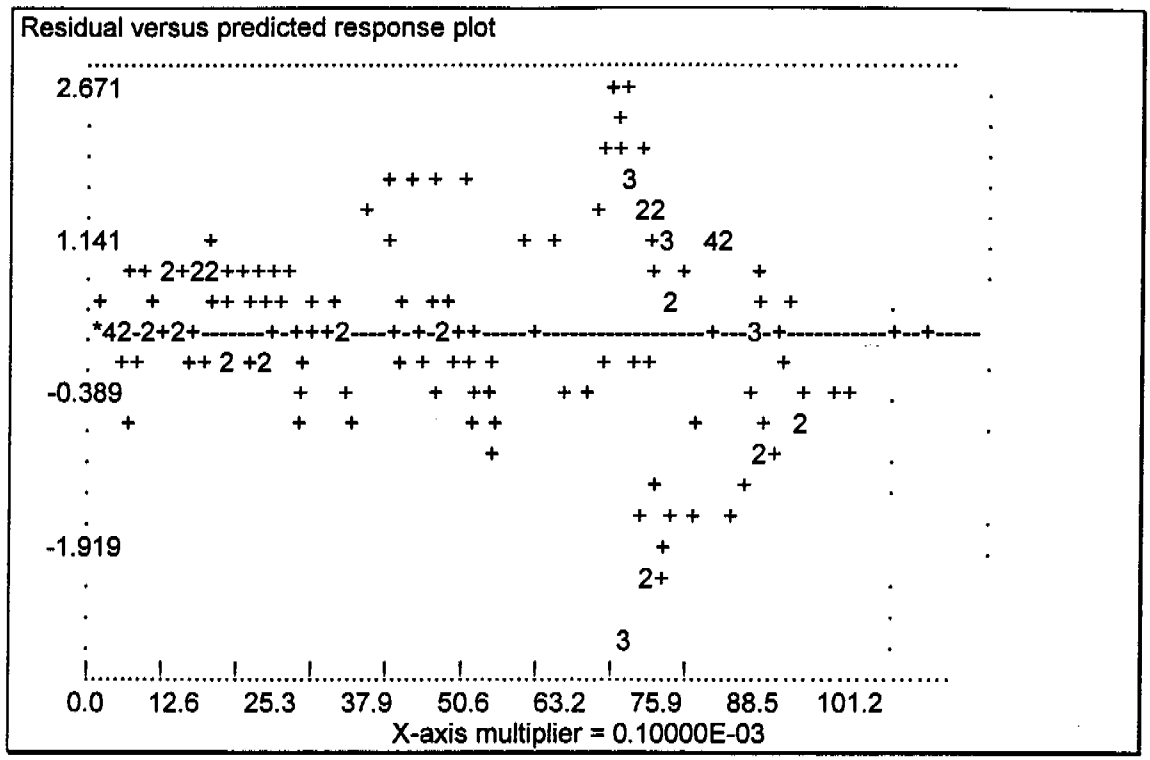

Figure 3.5.1: Plot of standardised residuals versus predicted response for a least squares model of the 1st January 1997 event. The increasing spread of standardised residuals versus predicted response indicates that the residual variance is increasing with predicted response thus violating the least squares model assumption. The number 'X' in this plot refers to 'X' residuals occupying virtually the same position.

It can be observed in Figure 3.5.1, that there is an increasing scatter of standardised residuals as the predicted response increases, indicating a violation of the least squares model. The corrections for violations of the simple residual plots are presented later in this Section.

Kuczera (1994) noted that a plot of time versus standardised residuals is useful for the detection of trends and periodicity in standardised residuals, and another tool for the evaluation of the adequacy of the least squares model. The number 'X' in the plot of standardised residuals versus predicted response (Figure 3.5.1), highlights that there are 'X' residuals occupying virtually the same position. Figure 3.5.2, illustrates a plot of time versus standardised residuals for the same storm event.

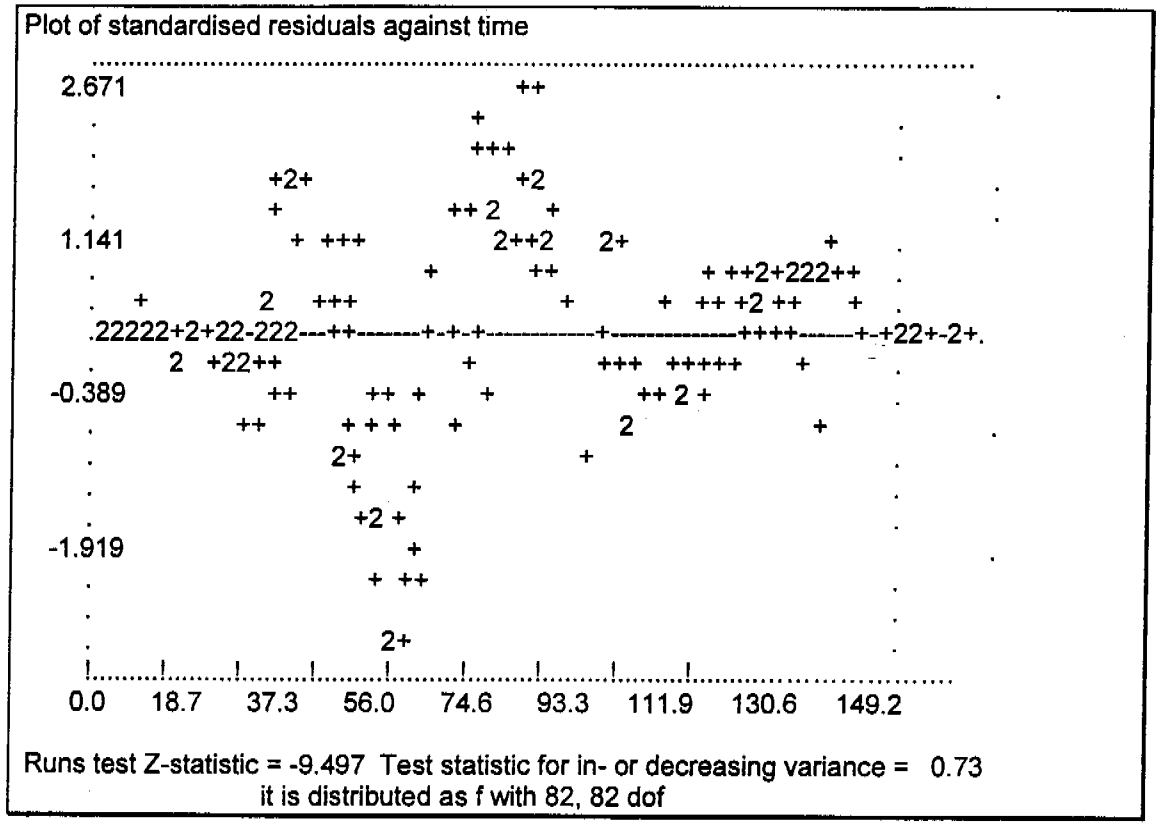

Figure 3.5.2: Plot of time versus standardised residuals for the 1st January 1997 event. The Z statistic being -9.5, exceeds the test value of |2|, indicating that the standardised residuals are not independent.

A pattern of scatter of increasing magnitude with time or the absolute value of the Z statistic exceeding 2 (as in the case of Figure 3.5.2), is an implication that the standardised residuals are probably not independent (Kuczera, 1994), a key assumption of the least squares model.

The normal probability of standardised residuals should, in a large sample, plot as a straight line, implying normality. The assessment of linearity is considered to be difficult (Kuczera, 1994), hence a Kolmogorov-Smirnov statistic and a 5% exceedance test value is used as an indicator of linearity. The normal probability plot for the 1st January storm event is presented in Figure 3.5.3.

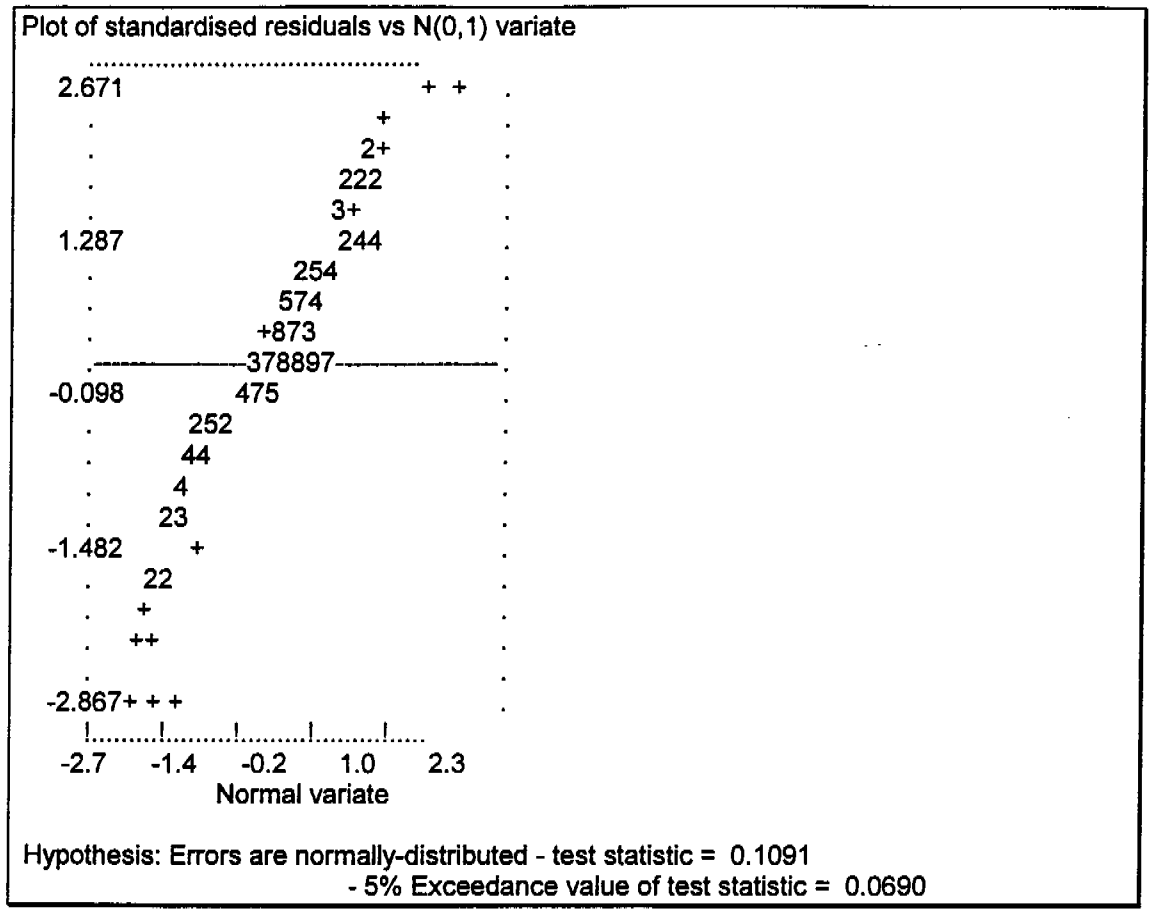

Figure 3.5.3: A normal probability plot for the storm event occurring on the 1st January 1997 with a Kolmogorov-Smirnov statistic of 0.1091, and a 5% exceedance value of 0.0690. As the Kolmogorov-Smirnov statistic exceeds the 5% test value, the residuals are considered not to be normally distributed.

If Kolmogorov-Smirnov statistic exceeds the 5% test value then it can be argued that the residuals are probably not normally distributed (Kuczera, 1994).

Plots of autocorrelation and partial autocorrelation give insight into the time dependence of standardised residuals. The 95% confidence limits on the autocorrelation function are represented by the dashed lines on Figure 3.5.4. Kuczera (1994) noted that if most of the autocorrelation plot falls inside the 95% limits, then the assumption that the standardised residuals are statistically independent is not inconsistent with the data.

Autocorrelation function

Lag	Autocorrelation	95% limits on white noise		-1.0 -.8 -.6 -.4 -.2 0.0 .2 .4 .6 .8 1.0
	Estimate			|....|....|....|....|....|....|....|....|....|....|
1	0.943	0.155	-0.155	< |***>**********
2	0.903	0.156	-0.156	< |***>**********
3	0.847	0.156	-0.156	< |***>*********
4	0.767	0.157	-0.157	< |***>********
5	0.689	0.157	-0.157	< |***>*******
6	0.608	0.158	-0.158	< |***>******
7	0.530	0.158	-0.158	< |***>*****
8	0.449	0.159	-0.159	< |***>****
9	0.367	0.159	-0.159	< |***>***
10	0.282	0.160	-0.160	< |***>**
11	0.209	0.160	-0.160	< |***>*
12	0.134	0.161	-0.161	< |***>
13	0.034	0.161	-0.161	< |* >
14	0.033	0.162	-0.162	< *| >
15	0.120	0.162	-0.162	<***| >

Note < and > denote approximate 95% limits on the white noise autocorrelation function

Figure 3.5.4: Residual autocorrelation plot for the 1st January storm event, which highlights the time dependence of the residuals, in this case the assumption of the residuals being statistically independent is not consistent with the data.

Divergence of residuals beyond the 95% prediction limits (Figure 3.5.4), suggests that an alternative to the least squares error model should be used. The partial autocorrelation plot from the storm event occurring on the 1st January is not presented.

Figure 3.5.5 highlights a cumulative periodogram plot for the 1st January storm event, which is analogous to the normal probability plot, but is particularly sensitive to periodicities in standardised residuals with constant variance (Kuczera, 1994).

Kuczera (1994) noted that although the theoretical periodogram should be a straight line assuming that the residuals are independent and constant, but for small samples, the plot deviates from the straight line due merely to sampling variability. The sample space was considered sufficiently large, so Figure 3.5.5 implies another violation of the least squares error model assumptions.

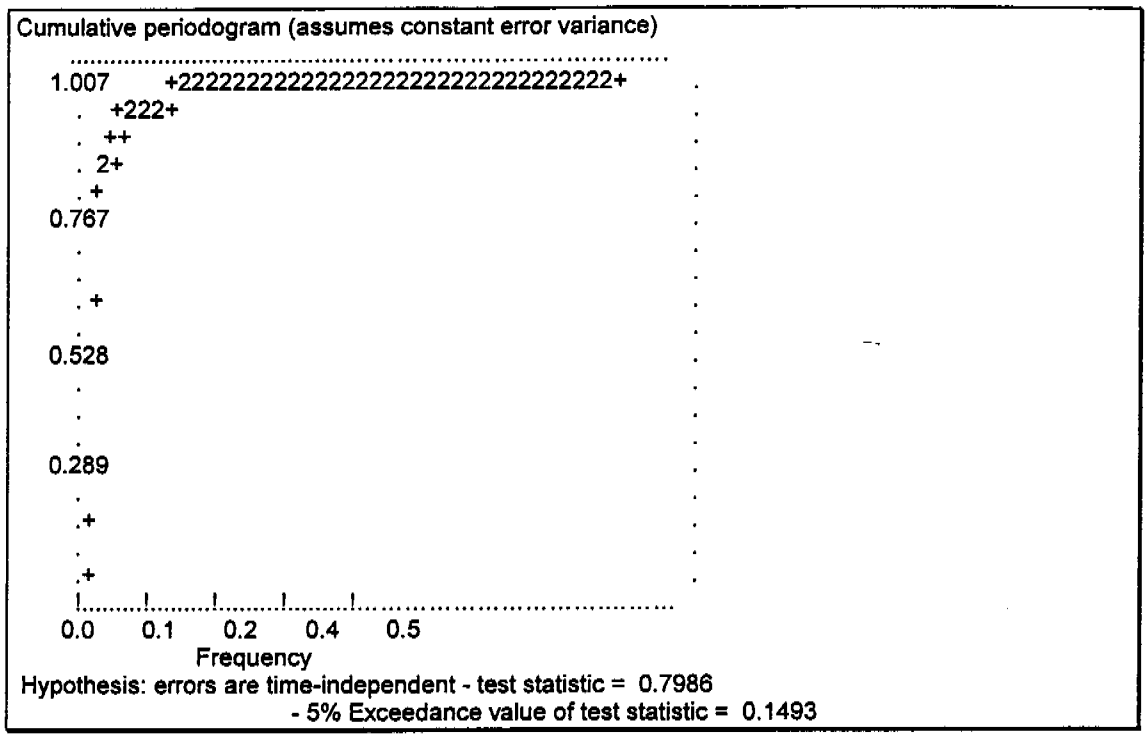

Figure 3.5.5: Residual cumulative periodogram plot for the 1st January 1997 storm event, which should be linear assuming that the residuals are independent and constant (an assumption of the least squares error model).

Kuczera (1994) noted that when the least squares model is invalidated, two options in NLFIT, in the form more general error models, can be employed to modify the errors so that the residuals conform more adequately with the least squares assumptions;

- To correct for non-stationary residual variance, when the scatter of the standardised residual versus predicted response plot is not in a uniform band, a Box-Cox transformation can be used. The Box-Cox model transforms the data in such a way that the variance of the random error and the transformed error are constant. Stabilisation of the residual variances often induces normality in the residuals (Kuczera, 1994).
- Kuczera continued that if the diagnostic plots infer a time dependence, then a complex ARMA (Auto Regressive Moving Average) time series model may be employed for correction.

3.6 Data

Natural rainfall event monitoring over the 1996/1997 wet season resulted in the accumulation of rainfall, runoff, and sediment loss data from numerous storm events. The raw hydrological data was transformed into DISTFW rainfall, runoff, and Field Williams files, and listed in Appendix 3.A (as previously reported in Section 3.3).

Table 3.6.1 lists the storm events (designated by the date of occurrence), the total rainfall recorded, (mm), the peak discharge, (L/s), and the approximate duration of the storm, (hours).

Table 3.6.1: Recorded storm events during the 1996/1997 wet season with associated total rainfall, (mm), peak discharge, (L/s) and storm duration (hours).

Storm Event.	*Total Rainfall, mm.*	*Peak Runoff, L/s.*	*Duration, hours.*
1/1/97	70.2	11.00	1.90
3/1/97[a]	58.4	6.00	4.90
3/1/97pm[a]	14.4	0.90	4.10
4/1/97	12.2	1.30	3.90
11-12/1/97	37.6	3.50	4.10
12/1/97[a]	5.0[b]	0.25	0.10
12/1/97pm[a]	16.5[b]	0.55	0.55
17/1/97	29.6	0.35	1.50
19/1/97	19.6	0.60	1.90
21/1/971st,[c]	11.8	0.40	0.77
21/1/972nd,[c]	22.4	1.70	1.50
22/1/97	30.8	0.70	8.20
23/1/97	43.8	12.00	2.60
23-24/1/97	40.6	3.00	6.30
28/1/97	28.2	2.50	4.00
19/2/97	64.6	1.20	4.50
20/2/97	32.4	4.00	2.20
22/2/97	29.0	4.00	3.50
22/2/97pm	26.8	3.70	4.20
23/2/97	23.0	3.30	4.10

[a] Afternoon and morning storm events occurred.
[b] No cumulative rainfall was available due to electronic raingauge failure.
[c] Two afternoon events.

It can be observed from Table 3.6.1, that there was considerable variation in the magnitude of rainfall events experienced during the monitoring season, with peak discharges ranging from 0.25 to 11 L/s. The cumulative rainfall listed in Table 3.6.1, although of similar magnitude, differed significantly with respect to intensity. Surface runoff from the field plot was observed to continue for a considerable period of time after the cessation of rainfall. The storm durations listed in Table 3.6.1, refer to the cessation of surface runoff, not the cessation of rainfall.

The DISTFW model required the input of the rainfall and runoff data for each storm event (Section 3.3), selection of appropriate initial estimates of parameter values (Table 3.4.1), and the choice of an error model. In all cases the "least squares" error model was chosen initially and a more general error model was selected in subsequent runs based on the results from the simple diagnostic residual plots produced as an output from the modelling process, and summarised for each storm event in Appendix 3.A. The output from the DISTFW-NLFIT model that was of primary interest in the current study was the mean and standard deviations of the kinematic wave parameters C_r and e_m and the infiltration parameters S_ϕ, and ϕ.

All storm durations listed in Table 3.6.1, were fitted with the DISTFW model utilising various error models and appear in Appendix 3.A in the form of Figure 3.6.1. Featured in Figure 3.6.1, is a plot of the cumulative rainfall, (mm), the observed hydrograph, (m^3/s), and the hydrograph predicted by DISTFW, (m^3/s), for a storm event occurring on the 1st January 1997.

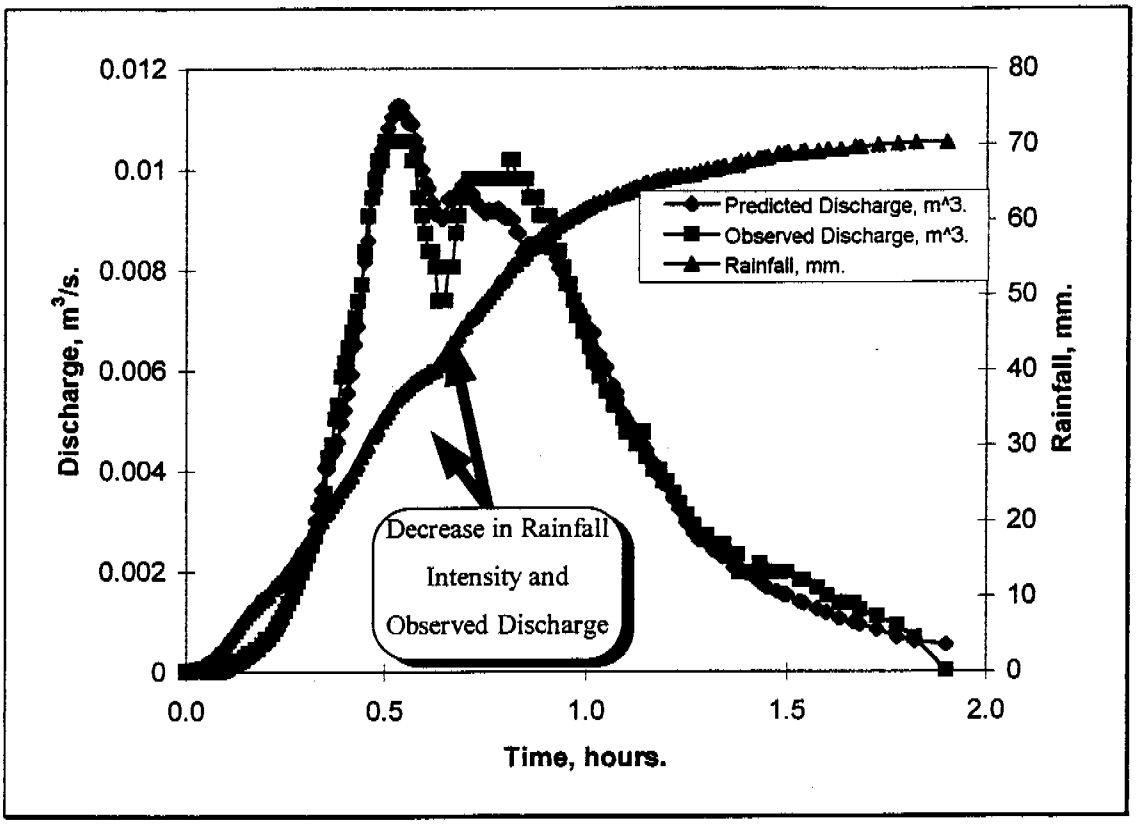

Figure 3.6.1: Observed and predicted discharge, (m^3/s), and cumulative rainfall, (mm), for the storm event occurring on the 1st January 1997. The large arrow indicates a reduction in rainfall that resulted in a subsequent decrease in observed and predicted discharge from the field plot.

Figure 3.6.1 highlights that the predicted hydrograph is very similar to that which was observed, especially in the incline and recession limbs. The over-prediction of the first peak and the under-prediction of the second peak is only of a minor concern. The large arrow in Figure 3.6.1 that is pointing towards the cumulative rainfall curve, indicates a slight reduction in rainfall intensity at the three-quarters of an hour mark after the commencement of rainfall. Corresponding to the slight reduction in rainfall intensity is the slightly delayed dip in surface runoff, yet as the rainfall re-intensifies, discharge increases accordingly.

Table 3.6.2 illustrates the kinematic wave and infiltration parameter values and their corresponding standard deviations for a select number of fitted storm events which fulfilled the criteria of the peak discharge exceeding 1 L/s (Willgoose pers. comm.) and a well defined storm duration. Storm events with discharge peaks less than approximately 1L/s, were considered to be non-significant events, when compared to events with discharge peaks ten times larger, for example the first event on 21st January with a peak of 0.4L/s, compared to the event on the 22nd February with a peak of 4L/s. The prediction of the discharge hydrograph, compared to that which was observed, for storm events with peak discharges less than 1L/s was generally much poorer than those storm events with peak discharges in excess of 1L/s. Comparisons between storm events can be made by consulting Appendix 3.A.

Figure 3.6.2 illustrates the storm event occurring on the 23-24th January, which was considered to be an example of a storm event with an ill-defined duration.

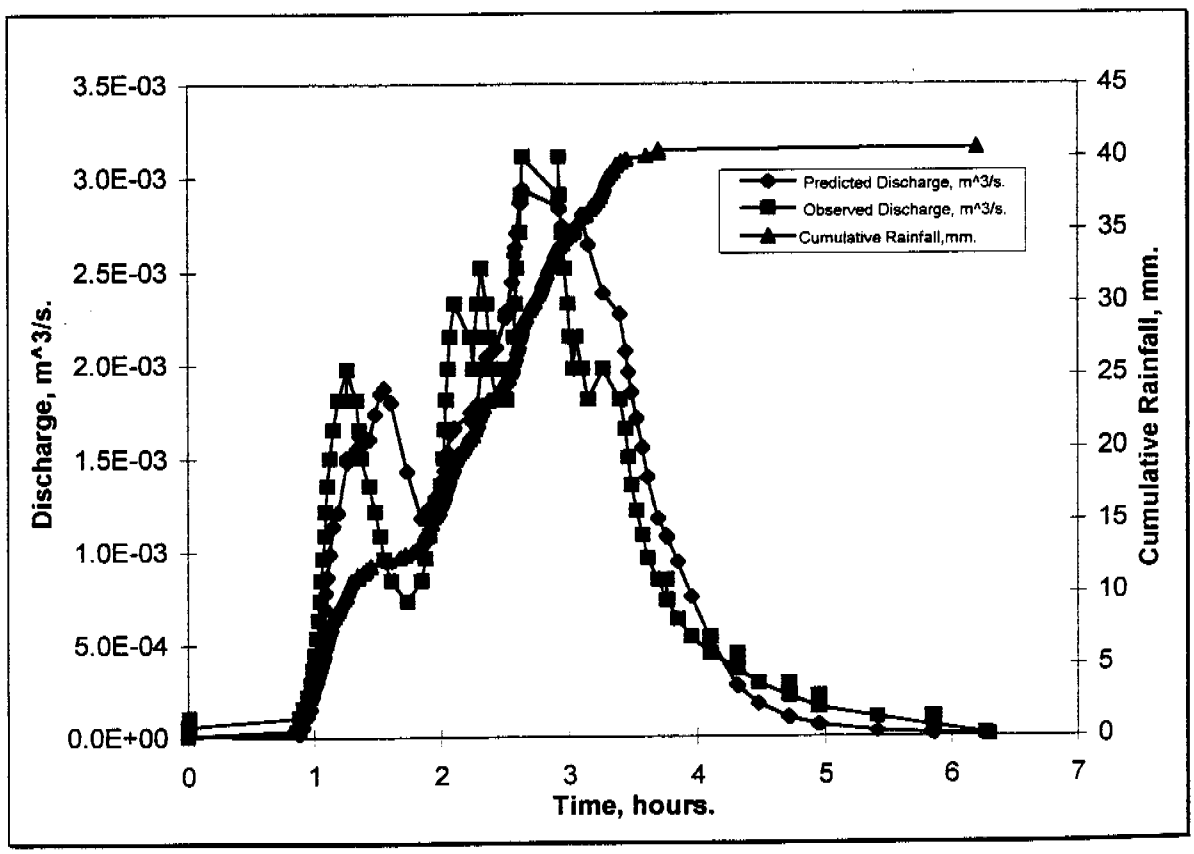

Figure 3.6.2: The ill-defined duration of the overnight storm event occurring over the 23rd-24th January, resulted in the considerable differences between the observed and predicted hydrographs.

The overnight storm event (Figure 3.6.2), involved only mild, drizzle-like rainfall for approximately four hours which resulted in considerable variation in the observed hydrograph, and hence was omitted from further analysis. Similar drizzle-like rainfall was prevalent for the overnight storm event occurring on the 11^{th}-12^{th} of January and was also omitted from further analysis.

Also featured in Table 3.6.2, is the error model utilised to obtain the best prediction of the runoff hydrograph compared to that observed. The utilisation of the auto-regressive model is summarised as 'AR', and the Box-Cox transformation model is summarised as 'BC'.

Table 3.6.2: Summary of infiltration and kinematic wave parameter values for all storm events that had a peak discharge in excess of 1L/s, and a definite storm duration.

Storm Event	*Error Model*	*Kinematic Wave Parameters*	*Mean (Standard Deviation)*	*Infiltration Parameters*	*Mean (Standard Deviation)*
1/1/97	1 AR BC=0.1	C_r	1.529(0.176)	S_ϕ (mm/hr$^{1/2}$)	7.825(0.715)
		e_m	1.631(0.091)	ϕ(mm/hr)	0.001
3/1/97	BC=0.1	C_r	4.001(0.668)	S_ϕ (mm/hr$^{1/2}$)	0.001
		e_m	1.554(0.081)	ϕ(mm/hr)	9.031(0.281)
4/1/97	Least Squares	C_r	6.775(0.152)	S_ϕ (mm/hr$^{1/2}$)	0.001
		e_m	1.291(0.096)	ϕ(mm/hr)	3.783(0.458)
21/1/972nd	BC=0.5	C_r	2.161(0.534)	S_ϕ (mm/hr$^{1/2}$)	14.997(8.211)
		e_m	1.513(0.153)	ϕ(mm/hr)	7.544(29.642)
23/1/97	Least Squares	C_r	2.257(0.109)	S_ϕ (mm/hr$^{1/2}$)	0.001
		e_m	1.596(0.051)	ϕ(mm/hr)	51.591(1.119)
28/1/97	Least Squares	C_r	9.168(1.083)	S_ϕ (mm/hr$^{1/2}$)	0.001
		e_m	2.697(0.083)	ϕ(mm/hr)	25.52(0.464)
19/2/97	Least Squares	C_r	0.631(0.097)	S_ϕ (mm/hr$^{1/2}$)	11.7(0.385)
		e_m	4.517(0.350)	ϕ(mm/hr)	0.001
20/2/97	Least Squares	C_r	3.211(0.505)	S_ϕ (mm/hr$^{1/2}$)	2.2578(1.913)
		e_m	2.093(0.189)	ϕ(mm/hr)	22.743(4.03)
22/2/97	Least Squares	C_r	4.312(0.537)	S_ϕ (mm/hr$^{1/2}$)	0.001
		e_m	2.104(0.085)	ϕ(mm/hr)	15.579(0.489)
22/2/97pm	Least Squares	C_r	11.62(2.005)	S_ϕ (mm/hr$^{1/2}$)	3.233(0.165)
		e_m	2.237(0.096)	ϕ(mm/hr)	0.001
23/2/97	Least Squares	C_r	6.110(0.788)	S_ϕ (mm/hr$^{1/2}$)	0.001
		e_m	2.077(0.103)	ϕ(mm/hr)	13.701(2.768)

The notation '1 AR',(Table 3.6.2), refers to the utilisation of a single auto-regressive factor, and the notation 'BC=0.5', refers to the use of a Box-Cox Lamba factor of magnitude 0.5. It should be noted that infiltrative parameters with a mean value of 0.001 with no standard deviation value in closed brackets in Table 3.6.2, refer to the scenario where the parameter was determined to be redundant by the NLFIT model. Large changes in a redundant parameter results in only minuscule changes in the objective function, and hence the magnitude of this parameter is irrelevant.

It can be observed from Table 3.6.2, that the magnitude of the kinematic wave parameters C_r, and e_m, for a few storm events are quite large. The relative magnitudes of the power term, e_m, of the conveyance function can be related to the various cross-sectional hillslope geometries discussed in Section 3.2.3. Several cross sectional areas were considered, with e_m values ranging from 1.67 to 1.21, for the constant depth over the entire width of the hillslope, case '*A*', to the irregular natural surface, case '*D*', respectively (Figure 3.2.5).

Willgoose (pers. comm.) noted that fitted storm events with e_m values well in excess of approximately 2.0 should be neglected, as e_m is a function of the geometric cross-sectional area and cannot realistically have such magnitudes. Two storm events were considered to have excessively high e_m values, 28th January (2.697) and 19th February (4.517), (Table 3.6.2). Examination of the observed versus predicted discharge output from the DISTFW model for the storm event on the 19th February, illustrates the unpredictable nature of the observed hydrograph which is believed to have resulted in the extraneous e_m value being obtained (Figure 3.6.3).

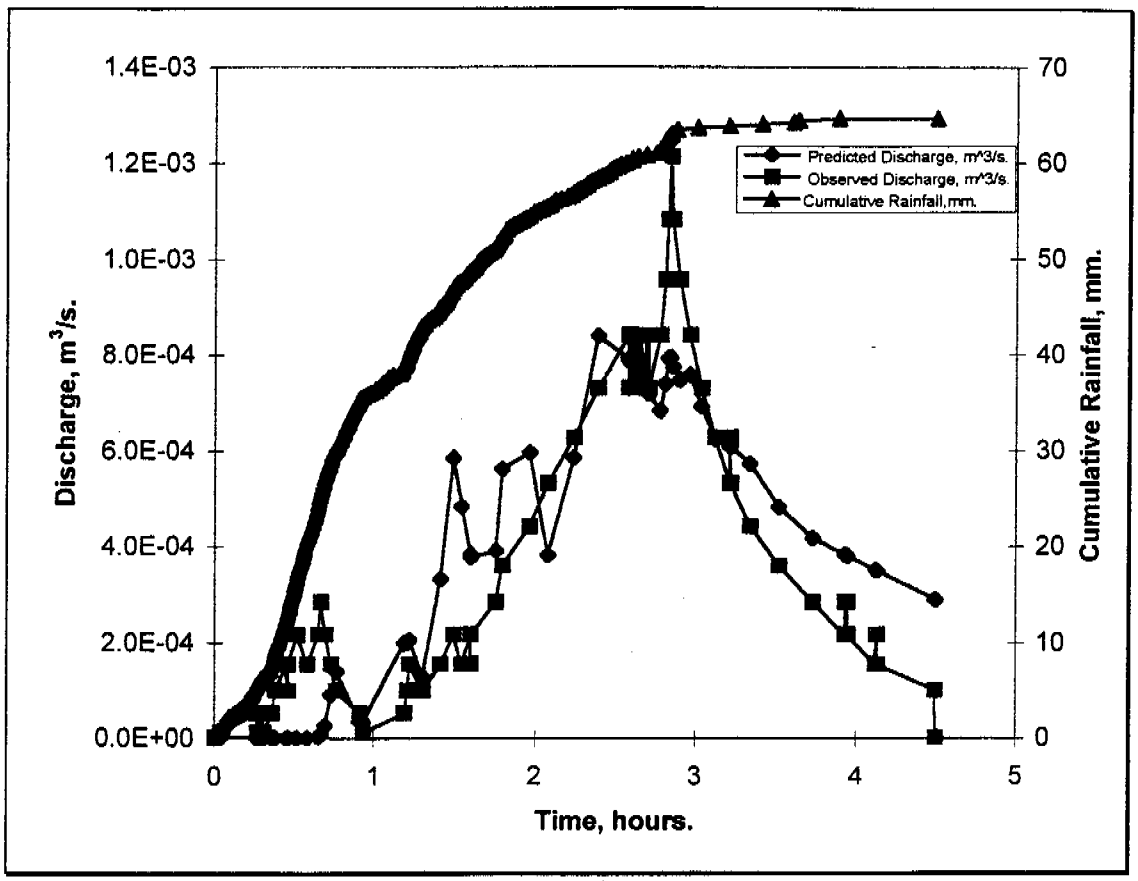

Figure 3.6.3: The predicted hydrograph of the storm event occurring on the 19th February, does not compare well with the observed hydrograph. Considerable fluctuation in the observed hydrograph over an extended period of time virtually negates the possibility of a smooth predicted response curve.

It can be observed from Figure 3.6.3, that the inclination and recession limbs, and the peak of the predicted hydrograph do not correspond well to the observed hydrograph. The considerable degree of fluctuation in the observed hydrograph is believed to be caused by fluctuating rainfall intensity.

The storm event occurring on the 28th January, although well fitted, Figure 3.6.4, has considerable fluctuation in the recession limb.

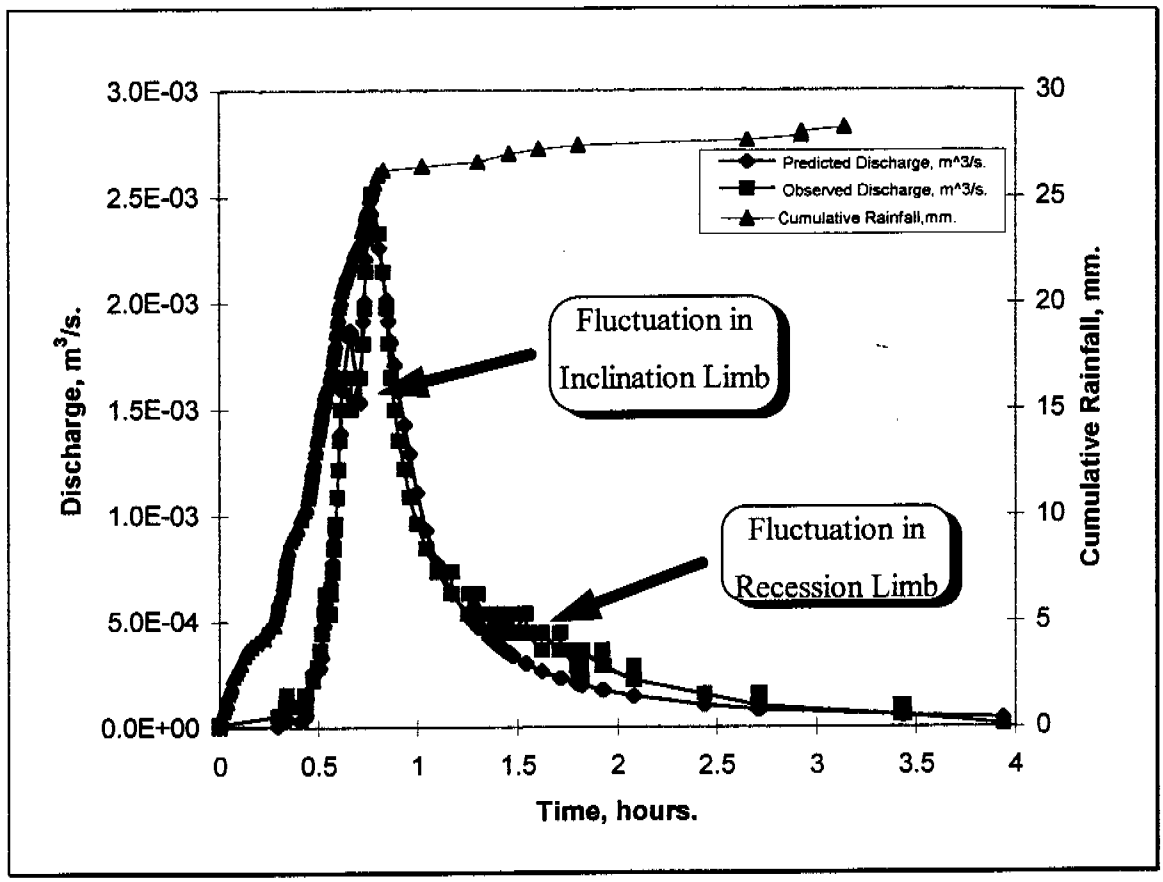

Figure 3.6.4: The inclination limb of the storm event occurring on the 28th January, is well estimated, with a slight drop in discharge resulting from a fluctuation in rainfall, highlighted by an arrow. The recession limb is dominated by fluctuations in the observed hydrograph, highlighted by an arrow, resulting from intermittent rainfall occurring at the 1.5 hour mark.

The arrows in Figure 3.6.4 highlight considerable fluctuation in the incline and recession limbs of the observed hydrograph which was surmised to have resulted in the extraneous e_m value of 2.667 being obtained from the DISTFW model.

The prediction of the runoff hydrograph for the second storm event occurring on the 21st January was considerably different from that which were observed. Figure 3.6.5 illustrates the plot of the cumulative rainfall, and the observed and predicted hydrographs for that storm event which was fitted with a Box-Cox error model.

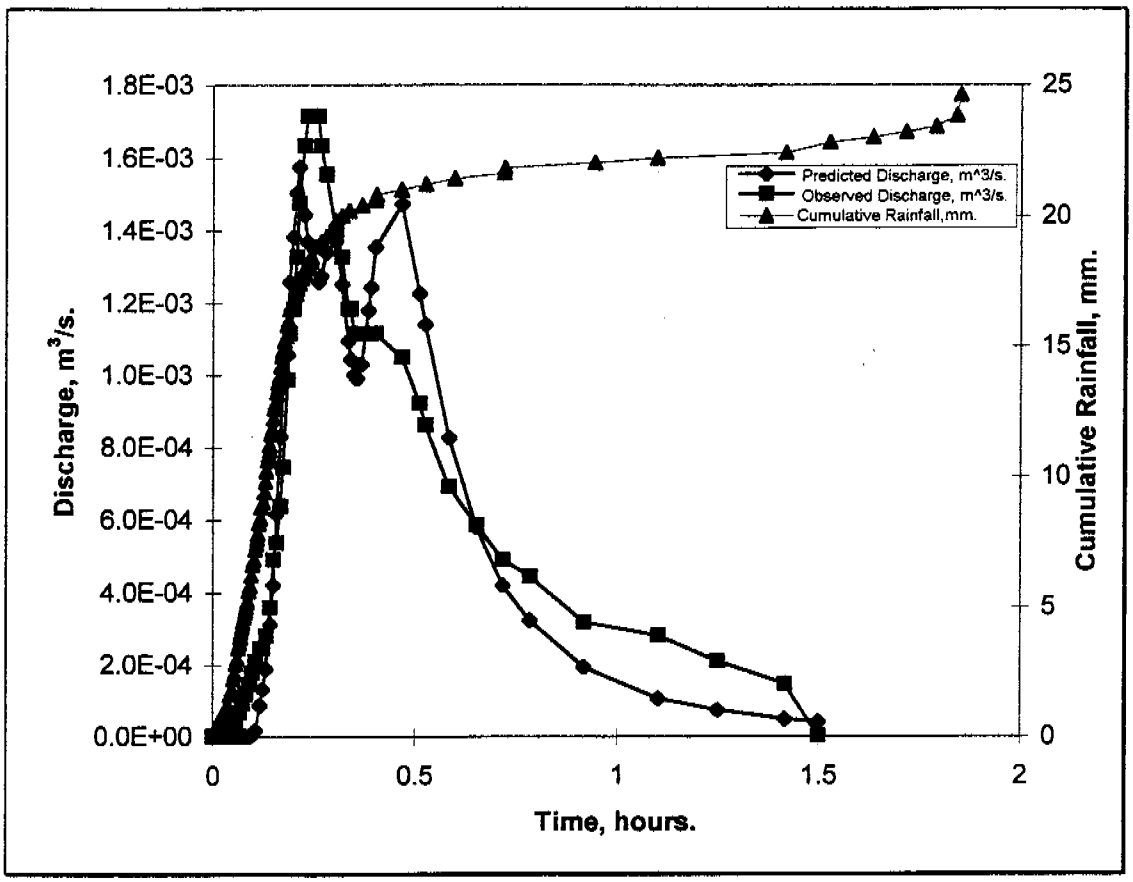

Figure 3.6.4: The inclination limb of the second storm event of the 21st January is adequately fitted, however the peak and the recession limb is poorly approximated. A large second discharge peak is predicted at the 0.5 hour mark and considerable under-prediction is evident beyond the 0.75 hour mark.

The predicted hydrograph for the second storm event occurring on the 21st January at the half and three-quarter hour marks, over-predicts and under-predicts respectively. This storm event was omitted from further analysis due to the poor predicted hydrograph compared to the prediction of hydrographs from other storm events.

3.7 Parameter Comparison

The DISTFW-NLFIT package has the ability to estimate parameters for a single rainfall event for a single site, or estimate one set of parameters to a number of events simultaneously at a single site (Saynor *et al*, 1995).

The surface storage parameters C_s and γ in the current study, were fixed permanently at 0.003 and 0.375 respectively, effectively disabling the surface storage component of the DISTFW model. In the analysis of the Tin Camp Creek data (Moliere *et al*, 1996), the same surface storage parameters values were chosen.

Moliere *et al* (1996) considered all the storm events that were fitted from data from the Tin Camp Creek study, and concluded the single fitted storm event(s), on the 30th December adequately represented all storm activity from both the Quartz and Mica sites. A module of the NLFIT program suite, PREDICT, enables the prediction of discharge for a sequence of storm events using the parameters fitted from a single event. The chosen parameters (in this case those estimated for the storm event(s) occurring on the 30th December), are considered adequate if more than 90% of the observed hydrograph data falls within the 90% prediction limits, plotted by the PREDICT module (Kuczera, 1994). This was the rationale utilised for the selection of the 30th December storm event as being representative.

Table 3.7.1 illustrates a comparison between the infiltrative and kinematic wave parameters from the current study for all the storm events listed in Table 3.6.2, (negating the three storm events referred to in Section 3.6) and the Tin Camp Creek study (Moliere *et al*, 1996).

Table 3.7.1: Mean and standard deviations for the kinematic wave and infiltrative loss DISTFW parameters for all the storm events from the current study listed in Table 3.6.2 (neglecting 22/1/97^{snd}, 23-24/1/97, and 28/1/97) and the Tin Camp Creek study (Moliere *et al*, 1996).

	Natural Site Pit No.1 ERARM	***Tin Camp Creek***			
		Representative Storm Quartz Site	Multiple Fitted Storm Quartz Site	Representative Storm Mica Site	Multiple Fitted Storm Mica Site
Parameter	Mean (Std.Dev.)	Mean (Std.Dev.)	Mean (Std.Dev.)	Mean (Std.Dev.)	Mean (Std.Dev.)
C_r	4.98 (3.22)	7.44 (1.12)	6.48 (0.56)	28.48 (35.12)	2.06 (0.32)
e_m	1.82 (0.34)	1.31 (0.05)	1.24 (0.03)	1.75 (0.32)	1.24 (0.04)
S_ϕ (mm/hr$^{1/2}$)	1.67 (2.79)	17.81 (0.78)	8.65 (0.12)	3.35 (1.50)	0.97 (0.39)
ϕ(mm/hr)	14.55 (16.95)	4.73 (0.50)	5.24 (0.26)	65.29 (5.24)	47.22 (1.98)

The multiple storms from the Quartz and Mica sites, referred to in Table 3.7.1, occurred on the 25th, 27th, 29th, and 30th of December 1993, are found in Moliere *et al*, (1996).

The representative storms referred to in Table 3.7.1 for the Quartz and Mica sites, are event(s) that occurred on the 30th December 1993, and can also be found in Moliere *et al*, (1996). Two storm events were monitored on the Quartz site on the 30th December, approximately two hours apart, whilst only one event was monitored on the Mica site. The relatively large standard deviations of both the kinematic wave and infiltrative loss parameters exhibited by the representative Mica site storm was due to the relatively poor fit of the observed hydrograph with respect to the peak and the volume of flow (Moliere *et al*, 1996).

The mean and standard deviations listed in Table 3.7.1 for the Tin Camp Creek study were produced from the DISTFW-NLFIT model. The mean and standard deviations reported in Table 3.7.1 for the current study, were produced from simple descriptive statistics of the estimated parameter values from eight individually calibrated storm events.

The standard deviation of the infiltrative loss parameters listed in Table 3.7.1 for the natural site are considerable, 2.79, and 16.95, for S_ϕ and ϕ, respectively. However, a large number of storm events, (five of the eight individually calibrated storm events) had redundant S_ϕ values, which were fixed at a value of 0.001. The standard deviation of ϕ for the natural site, although having fewer redundant values, (two of the eight individually calibrated storm events), was large with values ranging from 0.001 (redundant) to 51.59 mm/hr.

Considerable effort was taken to attempt to estimate a single set of parameters for a number of combinations of four storm events from the current study, to emulate what was undertaken in the Tin Camp Creek study. Large standard deviations, many orders of magnitude beyond the mean, were consistently obtained.

The inability to achieve reasonable estimations of a single set of parameters describing four storm events was believed to result from;

- Large differences in initial soil moisture conditions,
- Differences in rainfall intensities and durations, leading to different hydrological responses with respect to both hydrograph peaks and volumes, and
- Small uncertainties in the estimation of parameter values for individual events interacting to yield larger uncertainties in multiple storm parameter estimation.

Comparison of the hillslope routing and infiltrative properties of the natural site and the Mica and Quartz sites was undertaken utilising the COMPAT module of the NLFIT program suite.

The DISTFW-NLFIT program produces a posterior moments file (termed PMF files), which contains the mean and standard deviations of the parameters estimated in a correlation matrix. As a function of the COMPAT program, the Tin Camp Creek PMF's for the two sets of multiple storm events from the Mica and Quartz sites (Table 3.7.1), were not compatible with the single storm event PMF's produced from the current study. The number of parameters in the correlation matrix from the multiple storm sets from the Mica and Quartz sites totalled fifteen each, the seven parameters directly associated with the DISTFW model; C_r, e_m, C_s, γ, S_ϕ, ϕ, C_g, and a further eight parameters, (four lots of '*timing*' and '*initial wetness*' parameters for each storm event). As a set of multiple storm events could not be estimated for the current study, the single storm event PMF's (containing the seven parameters from the DISTFW model, and one set of '*timing*' and '*initial wetness*' parameters) were altered to include three extra sets of '*timing*' and '*initial wetness*' parameters to emulate a four storm set. The incorporation of the three 'dummy' storm events did not compromise the quality of the estimation of parameter values.

95% posterior probability plots from the module COMPAT, for the kinematic wave parameters, C_r and e_m, and the infiltrative loss parameters, S_ϕ, and ϕ, for the natural site and the Tin Camp Creek study were produced to evaluate the similarities between the data sets.

Two parameters are involved in each posterior probability plot, which are assumed for clarity of explanation to have a normal 'bell' shaped distribution with a certain mean and standard deviation. The combination of these two normal distributions, in three dimensional space, results in the formation of a mountain of posterior probability. The 95% probability ellipse is merely a plan view of the 95% slice of the three dimensional posterior probability mountain.

Any set of parameter values chosen from the data set under consideration has a 5% chance of falling outside the 95% probability ellipse. Each ellipse is thus an approximation to the actual region, which is increasingly accurate as the coefficient of variation of the parameters declines.

If the 95% probability ellipses for different data sets intersect, then the parameters in the data sets are considered not to be statistically different at the 5% level, implying compatibility. If a 95% ellipse of a single data set of two parameters is horizontal or vertical then it can be argued that the parameters are statistically independent of each other. A detailed evaluation of the statistical theory behind the COMPAT module of the NLFIT suite can be found in Kuczera, (1994).

The standard deviations for the redundant parameters reported in Table 3.7.2, were not obtained from the calibration procedure employed to obtain the results listed in Table 3.6.2. To adequately compare the infiltrative loss and kinematic wave parameters from the current study and the Tin Camp Creek study, the standard deviations of these redundant parameters were determined in a separate calibration series. Table 3.7.2 also lists the storm events that correspond to the numbered labels in Figure 3.7.1, which is a 95% posterior probability plot of the kinematic wave parameters, C_r and e_m.

Table 3.7.2: Summary of infiltration and kinematic wave parameter values for eight representative storm events from the natural site and from the Tin Camp Creek study.

Label Number	*Storm Event*	*Error Model*	*Kinematic Wave Parameters*	*Mean (Standard Deviation)*	*Infiltration Parameters*	*Mean (Standard Deviation)*
1	*1/1/97*	Least Squares	C_r	1.684 (0.081)	S_ϕ (mm/hr$^{1/2}$)	7.948 (1.525)
			e_m	1.675 (0.083)	ϕ(mm/hr)	0.280 (2.247)
2	*3/1/97*	Least Squares	C_r	4.480 (1.574)	S_ϕ (mm/hr$^{1/2}$)	0.245 (1.839)
			e_m	1.544 (0.199)	ϕ(mm/hr)	13.64 (2.071)
3	*4/1/97*	Least Squares	C_r	0.775 (0.137)	S_ϕ (mm/hr$^{1/2}$)	0.001 (214.54)
			e_m	1.291 (0.108)	ϕ(mm/hr)	3.783 (88.194)
4	*23/1/97*	Least Squares	C_r	2.258 (0.106)	S_ϕ (mm/hr$^{1/2}$)	0.001 (1867.6)
			e_m	1.596 (0.068)	ϕ(mm/hr)	51.58 (246.60)
5	*20/2/97*	Least Squares	C_r	3.211 (0.505)	S_ϕ (mm/hr$^{1/2}$)	2.258 (1.913)
			e_m	2.093 (0.189)	ϕ(mm/hr)	22.743 (4.03)
6	*22/2/97*	Least Squares	C_r	4.336 (0.506)	S_ϕ (mm/hr$^{1/2}$)	0.001 (124.55)
			e_m	2.108 (0.080)	ϕ(mm/hr)	15.541 (3.47)
7	*22/2/97pm*	1 AR BC=0.5	C_r	11.58 (2.402)	S_ϕ (mm/hr$^{1/2}$)	3.236 (0.689)
			e_m	2.236 (0.135)	ϕ(mm/hr)	0.001 (1.049)
8	*23/2/97*	Least Squares	C_r	6.110 (1.591)	S_ϕ (mm/hr$^{1/2}$)	0.001 (839.87)
			e_m	2.077 (0.246)	ϕ(mm/hr)	13.70 (593.17)
9	*Mica*	Least Squares	C_r	2.064 (0.321)	S_ϕ (mm/hr$^{1/2}$)	0.968 (0.393)
			e_m	1.242 (0.039)	ϕ(mm/hr)	47.225 (1.982)
10	*Quartz*	Least Squares	C_r	6.475 (0.562)	S_ϕ (mm/hr$^{1/2}$)	8.645 (0.122)
			e_m	1.242 (0.027)	ϕ(mm/hr)	5.238 (0.260)

It can be observed in Figure 3.7.1, that there is a well defined relationship between the kinematic wave parameters from the natural site, ellipses 1 to 8, Table 3.7.2. The Mica and Quartz sites, labelled explicitly in Figure 3.7.1, are quite similar in behaviour compared to the natural site. The Quartz site appears to be an outlier, however, differences in the geometry of the cross-sectional areas of flow were expected between the three different sites.

Storm events occurring towards the end of February generally had e_m values noticeably higher than events occurring at the beginning of the wet season. Figure 3.7.1, illustrates this trend with storm events labelled, 5 to 8, (20/2/97, 22/2/97, 22/2/97 pm, and 23/2/97) having a mean e_m value clearly above storm events 1 to 4 (1/1/97, 3/1/97, 4/1/97, and 23/1/97). Detailed consideration of the effect of vegetation growth across the field site is presented in Section 5.0.

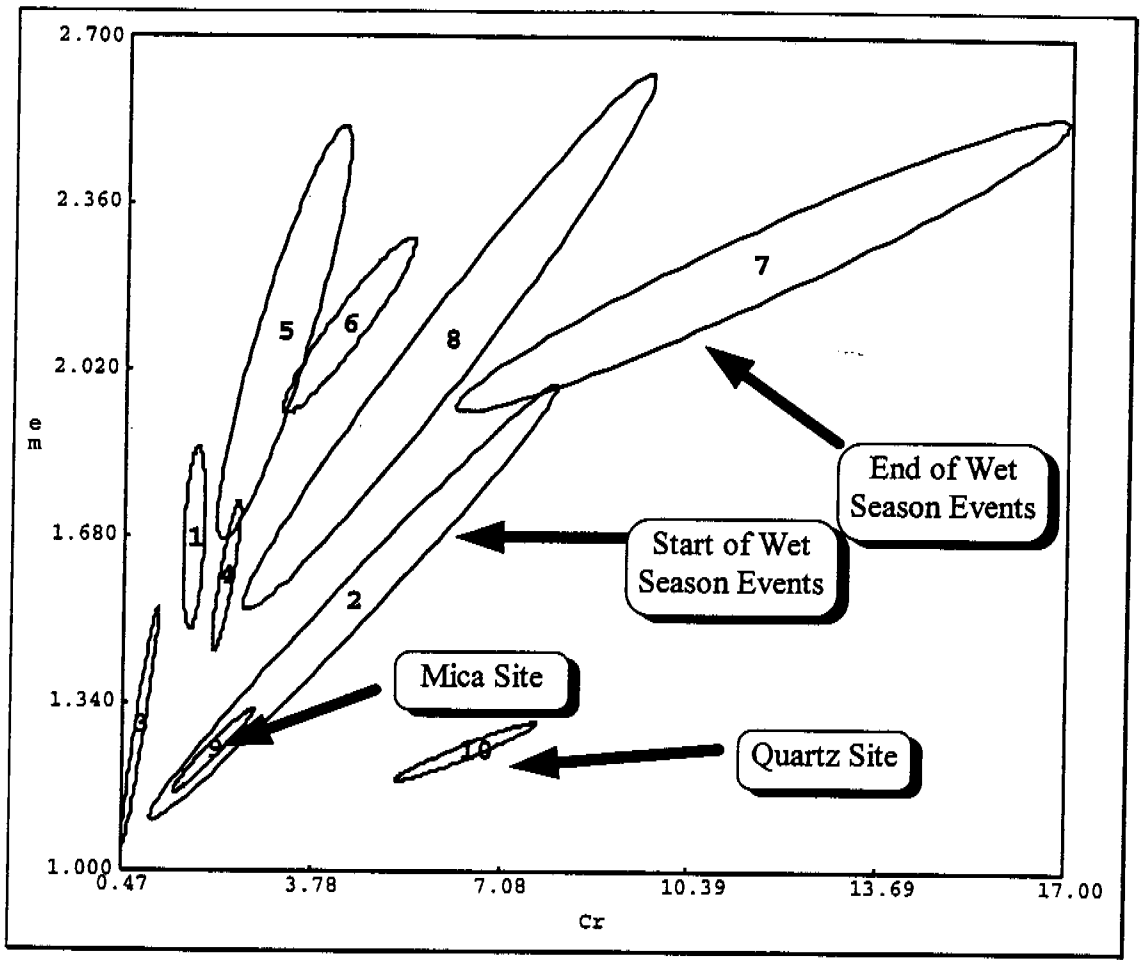

Figure 3.7.1: 95% posterior probability plot of the kinematic wave parameters, C_r and e_m, for the ten storm events listed from the current study and two parameter sets from the Mica and Quartz sites (Table 3.7.1).

The comparison of infiltrative parameters between the current study and the Mica and Quartz sites, utilising the same set of storms listed in Table 3.7.2, and displayed in Figure 3.7.1, was not conducted due to their considerable standard deviations. The DISTFW model, by producing large standard deviations for infiltrative parameters, is essentially stating that the volume of the hydrograph is very difficult to determine.

Storm events occurring on the 4th and 22nd of January and the 22nd and 23rd of February (listed in Table 3.7.2), had considerable standard deviations for infiltrative loss parameters and were examined individually, but omitted from further analysis. Figure 3.7.2, illustrates the predicted hydrograph from the storm event occurring on the 4th January.

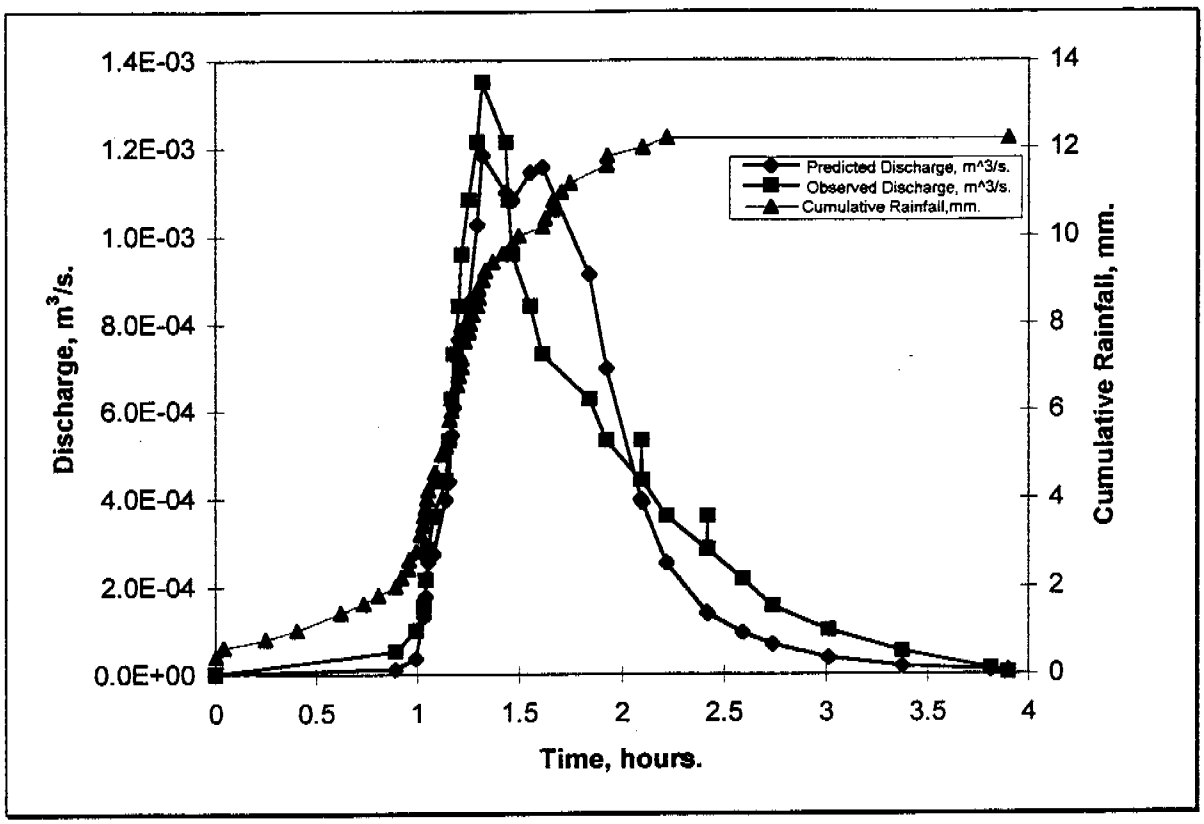

Figure 3.7.2: The predicted hydrograph for the storm event occurring on the 4th January, exhibits considerable deviation from the observed hydrograph in both the peak and the recession limb. Differences in the volume of the predicted hydrograph compared to that which was observed is believed to have been the origin of the large standard deviations of the infiltrative loss parameters listed in Table 3.7.2 for this event.

The storm event occurring on the 4th January had a peak discharge of only 1.30 L/s, which was the smallest of all storm events listed in Table 3.7.2 by at least 50 percent. Figure 3.7.2 highlights a poorly predicted hydrograph recession limb, which is believed to have resulted in the large standard deviations for the infiltrative loss parameters S_ϕ and ϕ, of 214.54, and 88.194, respectively (Table 3.7.2).

The peak discharge for the storm event occurring on the 23rd January was approximately 12 L/s, with a rainfall intensity of over 80mm/hour. The initial modelling attempt with DISTFW yielded a close fit between the predicted and observed hydrographs with a redundant initial loss (S_ϕ) parameter. A considerable amount of storm activity had occurred in the two days previous to this event, with two rainfall events occurring on the 21st January, and one ill-defined event occurring on the 22nd January which consisted of intermittent rainfall for a period of over eight hours. The large standard deviation of the S_ϕ parameter of 1867.6 (Table 3.7.2), illustrated the considerable uncertainty in the estimation of this parameter, which was believed to be a function of the unusually saturated soil conditions as a result of storm activity from the previous two days.

Figure 3.7.3 features the first storm event that occurred on the 22nd February. The cessation of the observed hydrograph is at approximately 3.25 hours, yet it has a non-zero discharge. The lack of hydrograph completion was caused by an error in the definition of the number of data lines in the DISTFW runoff file which prematurely cut off the end of the hydrograph. The non-zero end of the hydrograph caused problems as DISTFW attempted to estimate a virtually infinite hydrograph volume, which was translated into the relative large standard deviations for the parameters S_ϕ and ϕ, of 214.54, and 88.194, respectively (Table 3.7.2).

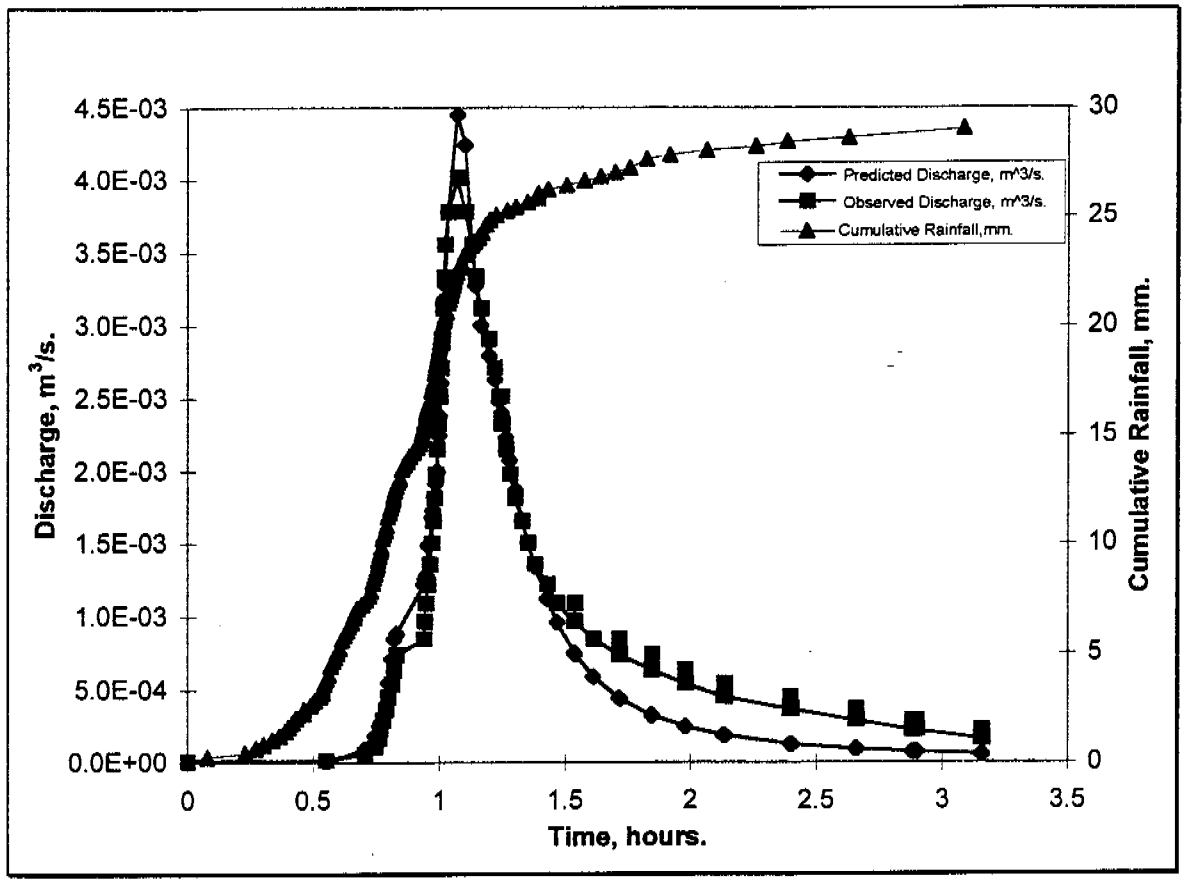

Figure 3.7.3: The end of predicted hydrograph for the storm event occurring on the 22nd February was non-zero, due to an error in the DISTFW runoff input file. This was believed to have resulted in difficulties in the estimation of the volume of the hydrograph which was translated into large standard deviations for the infiltrative loss parameters, S_ϕ and ϕ.

The storm event that occurred on the 23rd February (Figure 3.7.4), exhibited considerable fluctuation in rainfall intensity resulting in considerable corresponding fluctuation in the observed hydrograph. Large differences were noted between the predicted and observed hydrographs which was believed to be the origin of the large standard deviations for the infiltrative loss parameters, S_ϕ and ϕ, of 839.87, and 593.17, respectively (Table 3.7.2).

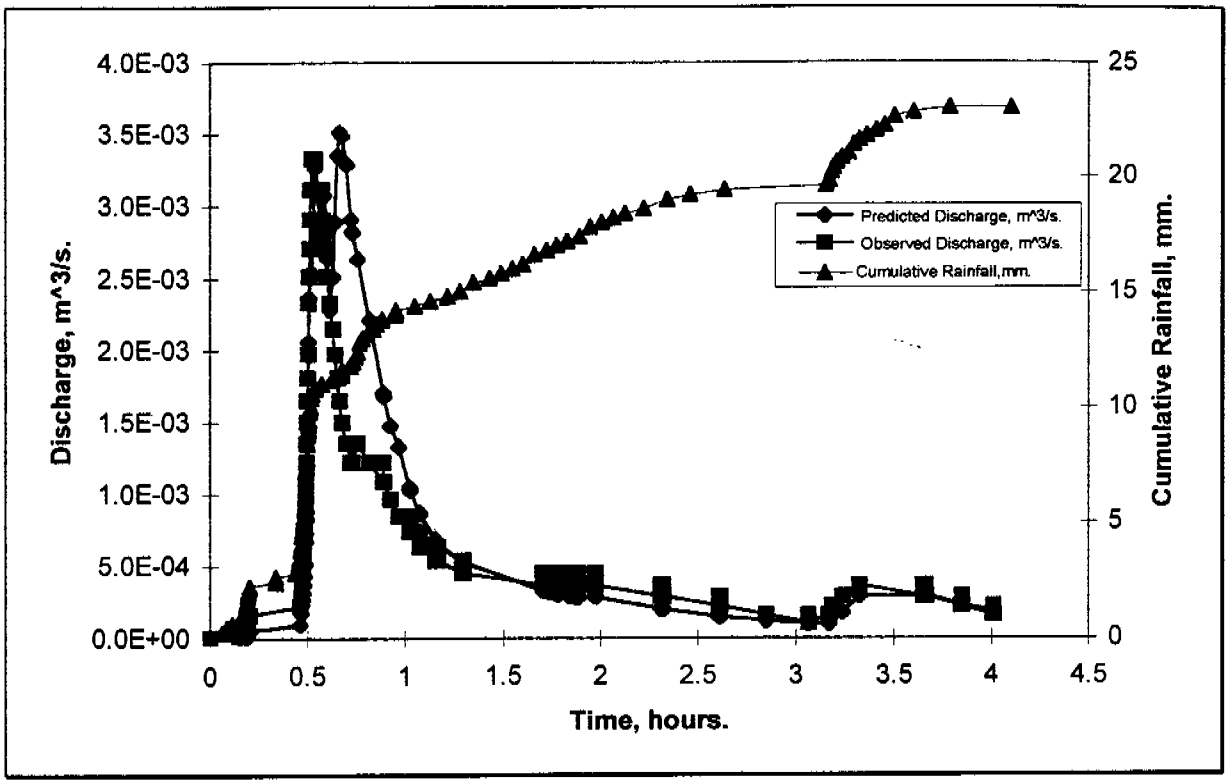

Figure 3.7.4: The predicted hydrograph for the storm event occurring on the 23rd February, exhibits considerable deviation from the observed hydrograph in both the peak and in the recession limb. Differences in the volume of the predicted hydrograph compared to that which was observed is believed to be the origin of the large deviations of the infiltrative loss parameters, S_ϕ and ϕ.

The 95% posterior probability plot of the infiltrative loss parameters, S_ϕ and ϕ, for the current study (neglecting storm events occurring on the 4th, and 23rd January, and 22nd and 23rd February), and the Mica and Quartz sites is presented as Figure 3.7.5.

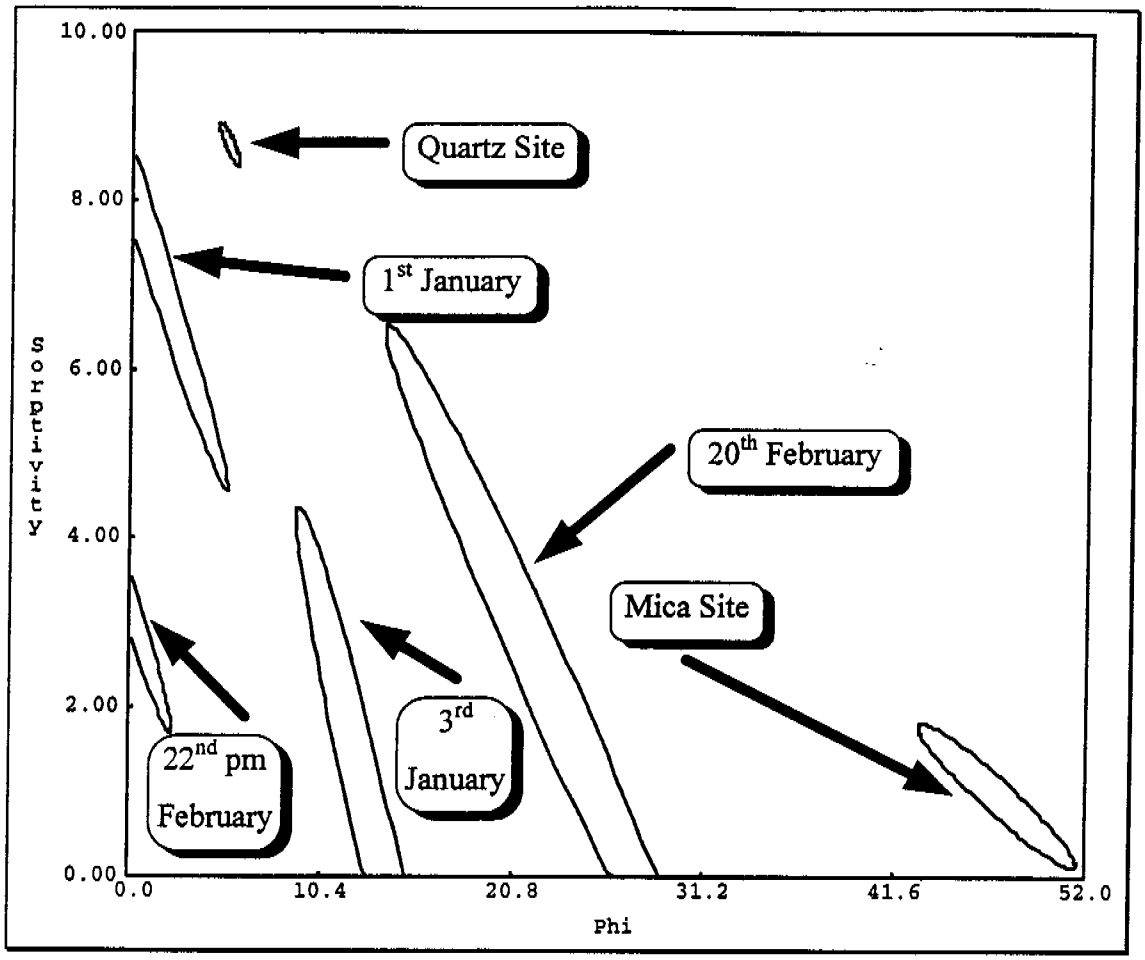

Figure 3.7.5: 95% posterior probability plot of the infiltrative parameters, S_ϕ and ϕ, for four storm events from the natural site, 1st and 3rd January, 20th and 22nd pm February, and the Quartz and Mica sites from Tin Camp Creek.

It can be observed in Figure 3.7.5, that the Mica site appears to not conform to the general trend exhibited by the remainder of the storm events from the natural site, and the Quartz site.

In conclusion, the Quartz site was not considered to be significantly different from the C_r and e_m parameter values, (Figure 3.7.1), from the current study and the Mica site. The Mica site however, was considered to be significantly different from the S_ϕ and ϕ parameter values, (Figure 3.7.5), from the current study and the Quartz site.